2004

Synthysis of polymer/nano-droplet composites from reverse microemulsion polymerization

Liehui Ge
liehui@rice.edu

SYNTHYSIS OF POLYMER/NANO-DROPLET COMPOSITES FROM REVERSE MICROEMULSION POLYMERIZATION

by

Liehui Ge

Thesis

Submitted to the School of Engineering Technology

College of Technology

Eastern Michigan University

in partial fulfillment of the requirements

for the degree of

MASTER OF SCIENCE

in

Polymer and Coating Technology

Thesis Committee:

John Texter, PhD, Chair

Weidian Shen, PhD

October, 2004

Ypsilanti, Michigan

SYNTHYSIS OF POLYMER/NANO-DROPLET

COMPOSITES FROM REVERSE MICROEMULSION POLYMERIZATION

by

Liehui Ge

APPROVAL:

John Texter, PhD	Date
Thesis Advisor and Chair	
Weidian Shen, PhD	Date
Committee Member	
Bob Lahidji, PhD	Date
Department Head	
Robert Holkeboer, PhD	Date
Associate Vice President for Graduate Studies and Research	

ACKNOWLEDGEMENTS

The author wants to extend special thanks to Dr. John Texter for his guidance and support throughout the course of this work.

The author is grateful to all committee members for all the efforts and time they spent on reviewing this thesis.

The author is forever indebted to his parents for their love and support.

ABSTRACT

L_1 and L_2 domains of the water/AOT/MMA ternary system were investigated at 22±1°C. Free radical polymerizations were conducted in L_2 domain. Only opaque polymer rods were obtained. Acrylamide, a water soluble monomer, plays a role of co-surfactant which greatly expands the L_2 domain. However, polymerizations only yielded opaque material. SEM showed images of phase separation.

MDOS (2-Methacryloyloxy)ethyl trimethylammonium bis(2-ethylhexyl) sulfosuccinate, was synthesized by ion exchange method. L_1 and L_2 domains of the water/MDOS/MMA ternary system were also investigated at 22±1°C. Free radical polymerizations were conducted in L_2 domain. Transparent polymer was produced. The "L_2" domain after polymerization was almost as large as L_2 domain. Polymerizations with acrylamide in the aqueous phase also produced transparent copolymer with up to 14% water. Polymer materials so produced were characterized by TGA, DSC, SEC, SEM.

TABLE OF CONTENTS

ACKNOWLEDGEMENTS		iii
ABSTRACT		iv
LIST OF FIGURES		ix
LIST OF TABLES		xv
ABBREVIATIONS		xvi
CHAPTER 1	Introduction and Background	1
	Reference	8
CHAPTER 2	Experimental	10
2.1	Materials	10
2.2	Methods	11
2.2.1	Preparation of Surfactants	11
2.2.2	Phase Diagram Mapping	13
2.2.3	Conductivity	16
2.2.4	Polymerizations of Reverse Microemulsion Systems	17
2.2.5	Thermogravimetric Analysis	18
2.2.6	Molecular Weight Analysis	18
2.2.7	Differential Scanning Calorimeter	19
2.2.8	Scanning Electron Microscopy	20
	Reference	21

CHAPTER 3	Surfactants.....	22
3.1	AOT.....	22
3.2	Preparation of 2-Methacryloyloxy)ethyl rimethylammonium Bis(2-ethylhexyl) sulfosuccinate.....	24
3.3	Preparation of 2-(acryloyloxy)ethyl trimethylammonium bis(2-ethylhexyl)sulfosuccinate.....	28
3.4	Preparation of Ag(AOT).....	29
3.5	Preparation of $Zn(AOT)_2$.....	32
3.6	Preparation of Sodium bis(2-ethylhexyl) phosphate.....	33
3.7	Preparation of 11- Acryloyloxyundecyl trimethylammonium bromide.....	34
	Reference.....	36
CHAPTER 4	Phase Diagrams.....	37
4.1	Partial Phase Diagram of WWATER/AOT/MMA System and Conductivity Studies.....	37
4.1.1	Phase Diagram.....	37
4.1.2	Conductivity.....	43
4.2	Partial Phase Diagram of Aqueous Acrylamide/AOT/MMA Systems	46
4.3	Partial Phase Diagram of Water/MDOS/MMA.....	52

4.4	Phase Diagram of 10 and 20 wt% Aqueous Acrylamide /MDOS/MMA Systems.....	54
4.5	Phase Diagram of Water/MDOS/MMA Systems with EGDMA and/or HEMA.....	57
	Reference.....	62
CHAPTER 5	Polymerization of AOT Systems and Characterizations.....	63
5.1	Polymerization.....	63
5.1.1	Polymerization in L_2 Domain of Water/AOT/MMA System.....	63
5.1.2	Polymerizations in 20% Aqueous caylamide/AOT/MMA System.....	69
5.2	Characterizations.....	70
5.2.1	Thermostability.....	71
5.2.2	Molecular Weight.....	74
5.2.3	Glass Transition Temperature.....	75
5.2.4	Thermoporosity Analyses by DSC.....	75
5.2.5	SEM Imaging.....	82
5.2.6	Ignition Test.....	85
	Reference.....	87
CHAPTER 6	Polymerization of MDOS Systems and Characterizations.....	88
6.1	Polymerization.....	88

6.1.1	Polymerizations in the L_2 Domain of Water/MDOS/MMA System.....	88
6.1.2	Polymerization in L_2 of Aqueous Acrylamide/MDOS/MMA System.....	94
6.1.3	Polymerization of Water/MDOS/(1:4 EGDMA:MMA) System.....	95
6.1.4	Polymerization of Water/MDOS/7:3 MMA:HEMA-5% EGDMA)	96
6.2	Characterizations.....	97
6.2.1	Thermostability.....	97
6.2.2	Molecular Weight.....	103
	Reference.....	108
CHAPTER 7	Conclusions and Future Work.....	109

LIST OF FIGURES

Figure	Brief Caption	Page
1.1	Schematic phase diagram of water/surfactant/oil ternary system	2
2.1	Visual titration path along a composition segment having constant surfactant/oil ratio	15
2.2	Visual titration path along a composition segment having constant surfactant weight fraction	16
3.1	Double-tail structure of AOT	22
3.2	TGA of AOT in air	24
3.3	Schematic ion-exchange mechanism	25
3.4	TGA of MDOS	27
3.5	Nominal structure of ADOS	28
4.1	Partial single-phase reverse microemulsion domain (L_2) of the water/AOT/MMA system	38
4.2	Single-phase microemulsion L_1 domain of the water/AOT/MMA system	40
4.3	Schematic phase diagram of the water/AOT/MMA system	41
4.4	Partial single-phase reverse microemulsion domain (L_2) of the water/AOT/MMA system	42

4.5	Paths where conductivity was studied	44
4.6	Log of conductivity vs. weight fraction of water	45
4.7	Partial single-phase reverse microemulsion domain (L_2) of the 5 wt% aqueous acrylamide/AOT/MMA system	47
4.8	Partial single-phase domain of the 10 wt% aqueous acrylamide system obtained at room temperature	48
4.9	Partial single-phase domain of the 20 wt% aqueous acrylamide system	49
4.10	Solubility of AOT increases with acrylamide weight fraction	51
4.11	Partial phase diagram of reverse microemulsion domain (L_2) of the water/MDOS/MMA system	52
4.12	Single-phase microemulsion domain (L_1) of the water/MDOS/MMA system	53
4.13	Partial phase diagram of the 0, 10, and 20 wt% aqueous acrylamide/MDOS/MMA systems	54
4.14	Partial phase diagram of the 10 wt% aqueous acrylamide/MDOS/MMA system	55
4.15	Partial phase diagram of the 10 wt% aqueous acrylamide/MDOS/MMA system	56
4.16	Partial phase diagram of the water/MDOS/1:4 EGDMA/MMA system	58
4.17	Partial phase diagram of the water/MDOS/7:3	59

	MMA:HEMA-5% EGDMA system	
4.18	Partial phase diagram of the water/MDOS/1:4 EGDMA:MMA system	60
4.19	Partial phase diagram of the water/MDOS/7:3 MMA:HEMA-5% EGDMA system	61
5.1	Loci of polymerization along the 30/70 AOT/MMA compositional segment	66
5.2	Polymerized AOT/PMMA samples	67
5.3	Loci of polymerization located in both L_2 and two-phase domains	68
5.4	Loci of polymerization on 15 wt% AOT path	69
5.5	TGA weight loss profiles for 30/70 AOT/PMMA samples with 0, 5 and 10 wt% water and a PMMA control.	71
5.6	TGA weight loss of samples produced at the composition illustrated in Figure 5.4	73
5.7	DSC data showing -11.75°C melting point depression for 10% water 30/70 AOT/PMMA sample.	76
5.8	Thermoporosity analysis for bottom part of 15% AOT 20/80 aqueous phase/MMA sample.	78
5.9	Thermoporosity analysis for top part of 15% AOT 20/80 aqueous phase/MMA sample	78
5.10	Thermoporosity analysis for bottom part of 15% AOT 40/60 aqueous phase/MMA sample	79

5.11	Thermoporosity analysis for top part of 15% AOT 40/60 aqueous phase/MMA sample	79
5.12	Thermoporosity analysis for bottom part of 15% AOT 50/50 aqueous phase/MMA sample	80
5.13	Thermoporosity analysis for top part of 15% AOT 50/50 aqueous phase/MMA sample	80
5.14	Thermoporosity analysis for 15% AOT 60/40 aqueous phase/MMA sample	81
5.15	Thermoporosity analysis for 15% AOT 80/20 aqueous phase/MMA sample	81
5.16	SEM image of Pt/Pd shadowed fracture surface for 15% AOT 0% water sample	83
5.17	Energy dispersive x-ray elemental analysis for the fractured surface	84
5.18	Ignition test results for 30/70 AOT/PMMA with 0, 5, 10% water, along with PMMA control and AOT	85
6.1	Schematic L_2 domain of water/MDOS/MMA system obtained at 70°C	89
6.2	Loci of reverse microemulsion polymerizations along the 20/80 and 40/60 MDOS/MMA.	91
6.3	MDOS/PMMA samples polymerized at 70°C. The compositions were formulated at 20/80 MDOS/MMA with 0, 5 wt% water	92

6.4	MDOS/PMMA samples polymerized 70°C. The compositions were formulated at 40/60 MDOS/MMA with 0, 5, and 10% water	92
6.5	MDOS L_2 domain that produces clear composites is nearly the entire L_2 domain in the water/MDOS/MMA system	93
6.6	Water-MDOS sample and 10% aqueous acrylamide-MDOS sample	95
6.7	40/60 MDOS/(7:3 MMA:HEMA with 5% EGDMA) samples formulated with 0, 5, 10, and 14% water photographed along with PMMA	97
6.8	Weight loss of 20/80 MDOS/PMMA samples with 5 wt% water in air	98
6.9	Weight loss 20/80 MDOS/PMMA samples with 5wt% water in N_2	100
6.10	Weight loss of polymerized 40/60 MDOS/(1/4 EGDMA/MMA) samples with 0, 5 and 10 wt% water in air	101
6.11	Weight loss of polymerized 50/50 MDOS/MMA with 14% water and 50/50 MDOS/MMA with 15.5% of 10% aqueous acrylamide in air	102
6.12	Log M_n for poly(MDOS/MMA) vs. MDOS weight fraction	105
6.13	Log M_w for poly(MDOS/MMA) vs. MDOS weight fraction	105

6.14 Log M_z for poly(MDOS/MMA) vs. MDOS weight fraction 106

6.15 Molecular weight distribution of poly(MDOS/MMA) 106

LIST OF TABLES

Table	Brief Caption	Page
3.1	MDOS elemental analysis results	26
3.2	ADOS elemental analysis results	29
3.3	Ag(AOT) elemental analysis results	32
3.4	$Zn(AOT)_2$ elemental analysis results	33
3.5	AUMAB elemental analysis results	35
5.1	Molecular weight analysis of polymer samples produced by polymerization of 30/70 AOT/MMA containing 0, 5, 10wt% water	74
5.2	Melting point depression data and porosity analyses for 15% AOT samples illustrated in Figure 5.4	77
6.1	Molecular Weight Analysis of PMMA Control and of MDOS/MMA Copolymers	103

ABBREVIATIONS

MMA	methyl methacrylate
BPO	benzyol peroxide
DDAMA	didecyldimethylammonium methacrylate
Na11-EAAU	11-(N-ethylacrylamido)undecanoate
AUTMAB	[(acryloyloxy)undecyl]trimethylammonium
AUDMAA	[(acryloyloxy)undecyl]dimethylammonio acetate
AOT	sodium bis(2-ethylhexyl)sulfosuccinate
PMMA	polymethylmethacrylate
EGDMA	ethyleneglycol dimethacrylate
TGA	thermogravimetric analysis
MDOS	2-methacryloyloxy)ethyl trimethylammonium bis(2-ethylhexyl) sulfosuccinate
DSC	differential scanning calorimeter
SEM	scanning electron microscopy
HEMA	2-hydroxylethyl methacrylate
AAM	acrylamide
MEHQ	hydro-quinone monomethyl ether
AIBN	2, 2'-azobisisobutyronitrile
MADQUAT	2-(Methacryloyloxy)ethyl trimethylammonium chloride

THF	tetrahydrofuran
ADOS	(2-acryloyloxy)ethyl trimethylammonium dioctylsulfosuccinate
SEC	Size Exclusion Chromatography
HFIP	1,1,1,3,3,3-hexafluoroisopropanol
CMC	critical micelle concentration
AUMAB	acryloyloxyundecyl trimethylammonium bromide
APS	ammonium persulfate

CHAPTER 1

INTRODUCTION AND BACKGROUND

Microemulsions are isotropic, thermodynamically stable, and optically transparent solutions of two immiscible liquids, stabilized by a surfactant and often with a co-surfactant. The term "microemulsion" was coincided about 15 years after Hoar and Schulman observed the spontaneous formation of a transparent "solution" of immiscible oil, water, and a surfactant with a co-surfactant. [1, 2] Microemulsions are macroscopically homogenous. At microscopic level, microemulsions are heterogeneous. Domains of varieties of micro-structures that exist are illustrated by a schematic phase diagram in Fig 1.1. Micro-structures have been determined are spherical droplets of oil dispersed in continuous water (oil-in-water, o/w or L_1 domain) and water droplets dispersed in oil (water-in-oil, w/o or L_2 domain). Radii of the micro-droplets are usually in the order of 10~100nm. The sizes of the droplets are really responsible for the transparency of microemulsions. Their sizes are often less than 1/20 of wavelength of visible light. [2-4] So, they do not scatter visible light. Bicontinuous structure may also exist, in which both water and oil domain are continuous. L_1 and L_2 domain are usually interconnected by bicontinuous domain. [5]

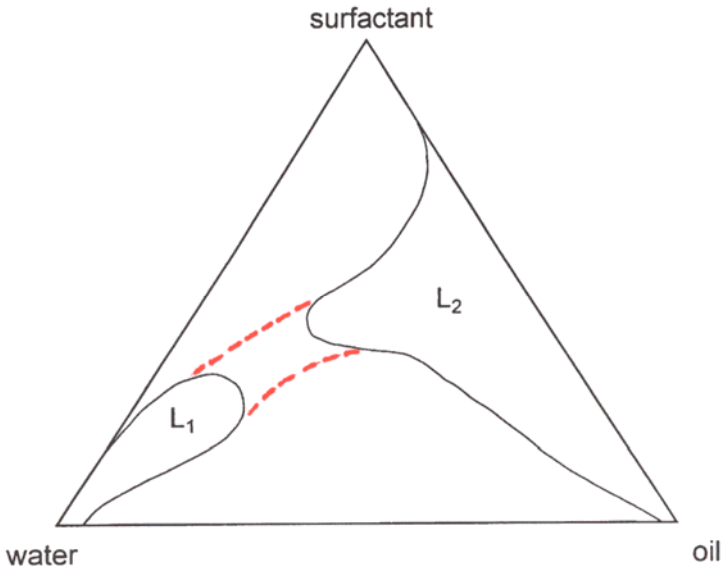

Figure 1.1 Schematic phase diagram of water/surfactant/oil ternary system. The region marked by the two dashed lines between L_1 and L_2 depicts bicontinuous microemulsion domain.

Due to the ability of microemulsions to form interesting micro-structures, the preservation of these micro-structures of water-in-oil microemulsion and bicontinuous microemulsion via polymerization has been one of the frontiers in making new materials, such as latexes, nanoparticles, nanocomposites, and porous membranes. The ability to preserve micro-structures of tunable topology and length scales has attracted much interest. Polymerizations have been attempted for essentially all possible types of microemulsions in order to preserve the original microstructure.[6-9] Water-in-oil microemulsions and bicontinuous microemulsions containing monomer(s) in the pseudo oil phase or aqueous phase or both, are of practical and theoretical interest for making polymer particles,

latexes and porous structures of having porosity on a nano-length scale, and for studies of the kinetics and mechanism of polymerization in reverse microemulsion systems.

UV light, γ radiation and oil and water soluble free radical sources have been used to initiate polymerization in reverse microemulsions. [10, 11] In the process of polymerization, due to temperature and composition changes, phase separation often happens and it is difficult to preserve or capture the original microstructure. [12, 13] Many attempts have been made to minimize or eliminate such phase separation. Three approaches have been attempted. One approach is to the increase polymerization rate. High conversion is achieved so that the microstructure is preserved before phase separation occurs. A second approach is to introduce cross-linking so that network structure forms at an early stage of polymerization. This network increases viscosity of the system and encumbers movement and collisions of the microstructures and this deceased movement slows phase separation. A third approach is to use polymerizable surfactant that can preserve the interfacial network of the microstructure during polymerization. [14] The use of polymerizable surfactant appears to be the most successful.

Many research groups reported that length scale of the micro-structures in the original single phase microemulsions were not preserved by using

non-polymerizable surfactants. And some of them also did polymerization with polymerizable surfactants. There have been a lot of reports of successes.

Mackay et al studied polymerizations in MMA/AOT/Water reverse microemulsion systems thermally initiated with benzyol peroxide at 55-60°C. [15] Only opaque products were obtained. Similar polymerizations were carried out in bicontinuous systems. Phase separation could be decreased by the use of cross-linking agents. However, the materials were still not transparent. The use of polymerizable surfactants were also studied and reported, either alone or in combination with cross-linking agent, in order to prevent phase separation during microemulsion polymerizations. Polymerization of water/MMA systems with didecyldimethylammonium methacrylate (DDAMA), a cation surfactant with polymerizable counter ion, instead of AOT, led to transparent solids with weak Tyndall scattering. But only a small clear domain after polymerization in the L_2 corner of water/DDAMA/MMA phase diagram was obtained (Figure 6.4) where the DDAMA concentration was no more than 20 wt%, and water contents were less than 3 wt%. Without water, clear co-polymers were obtained at DDAMA concentrations up to 35 wt%.

Gan et al reported bicontinuous microstructured transparent polymeric materials prepared from bicontinuous microemulsion polymerization.

Several types of transparent porous polymeric materials were successfully prepared from the polymerization of microemulsions containing polymerizable surfactants. Polymerizations of microemulsion systems with anionic sodium 11-(N-ethylacrylamido)undecanoate (Na11-EAAU) [16], cationic [(acryloyloxy)undecyl]trimethylammonium bromide (AUTMAB) [17, 18], and zwitterionic [(acryloyloxy)undecyl]dimethylammonio acetate (AUDMAA) [17] were investigated.

Cheung et al investigated the preparation of porous polymeric solids by the polymerization of monomer-containing microemulsions and the relationship between the microemulsion precursor structure and the polymer morphology was studied. [19] The effects of factors associated with precursor composition on the resulting polymeric solid morphology formed from thermally initiated polymerization have been supported.

A primary objective of our work is to develop a method to preserve the length scale of the water droplets in reserve microemulsion, so that transparency to visible light can be achieved during and after polymerization. Another objective is to investigate the fire resistance imparted by such incorporated water. Attempts have been made to map out the L_1 and L_2 domains of the water, AOT [sodium bis(2-ethylhexyl)sulfosuccinate], methyl methacrylate ternary system at 22±1°C, and to prepare polymer composites with a series of starting

reverse microemulsions within the L_2 domain and in the adjacent two phase emulsion region by free radical polymerization to produce polymethylmethacrylate (PMMA) with entrapped water droplets. However, only opaque polymer rods were obtained, even though the starting reverse microemulsions were transparent. The length scales, over which water-PMMA micro-phase separation occurs, decrease as water content and surfactant content decrease. Both water and surfactant appear to provide flame and ignition resistance. L_1 and L_2 domains of similar microemulsion systems with the hydrophilic monomer acrylamide in the aqueous phase and with or without the cross-linking agent ethyleneglycol dimethacrylate have been studied. The presence of acrylamide in the aqueous phase expands the L_2 domain towards the water corner. The L_2 and L_1 domains connect at 40/60 AOT/MMA when acrylamide is 20 wt%. Free radical polymerizations were also conducted with these systems. Only opaque or translucent rods with obvious evidence of micro-phase separation were recovered. Phase separation in all cases occurs at an early stage of polymerization, approximately 20 minutes after polymerization starts. TGA weight loss profiles of the opaque or translucent rods under nitrogen and air indicates water that is entrapped in is consistent with the compositions of starting inverse microemulsions. Perhaps phase separation is due to AOT being less soluble in polymer/monomer mixtures.

An approach to modifying AOT by replacing the sodium ion with a polymerizable cation has been investigated. A new surfactant with polymerizable cation and double-tail anion, MDOS (2-Methacryloyloxy)ethyl trimethylammonium bis(2-ethylhexyl) sulfosuccinate, has been synthesized by ion exchange methods.[20] Attempts have been made to map out the L_1 and L_2 domains for the water, MDOS, methylmethacrylate ternary system at 22±1°C. Free radical polymerizations have been conducted within L_2 domain and in the adjacent two phase emulsion domain in order to entrap water droplets. Optically transparent polymer composites with up to only 1~2 wt% water less of clear/turbid boundary of the L_2 domain have been successfully made. Translucent polymers were also obtained with a starting system in the adjacent two phase emulsion region. Compared with the water/AOT/MMA system, the length scales, over which water-PMMA phase separation occurs decrease dramatically. Also, cross-linking, hydrogel, and surfactant polymerization variations have been examined with a view towards further understanding of factors that control phase separation (and transparency) on meso- and nano-lengthscales. Similar polymerizations have been conducted with 10, and 20wt% aqueous acrylamide with 5 wt% cross-linking agent ethyleneglycol dimethacrylate. Transparent polymers are achieved in all cases with MDOS. TGA, DSC and SEM have been used to characterize the transparent polymer rods obtained.

REFERENCES

1. Schulman, J. H.; Cocknain, E. G. *Trans. Faraday Soc.* **1940**, 36, 661.
2. Hoar, T. P.; Schulman J. H. *Nature* **1943**, 152, 102.
3. Bowcott, J. E.; Schulman J. H. *Z. Elektrochem.* **1955**, 59, 283.
4. Schulman, J. H.; Stoekenius, W.; Prince, L. M. *J. Phycs. Chem* **1959**, 63, 1677.
5. Scriven, L. E. *Nature* **1976**, 263, 123.
6. Stoffer, J. O.; Bone, T. J. *J. Dispersion Sci. Technol.* **1980**, 1, 393.
7. Menger, F. M.; Tsuno, T.; Hommond, G. S. *J. Am. Chem. Soc.* **1990**, 112, 1263.
8. Palani, W. R.; Sasthav, M.; Cheung, H. M. *Polymer* **1995**, 26, 13, 2637.
9. Haque, E.; Qutubudin, S. J. *J. Polym. Sci.: Polym. Lett. Ed.* **1990**, 26, 429.
10. Li, T. D.; Gan, L. M.; Chew, C. H. *J. Membr. Sci.* **1997**, 133, 177.
11. Sasthav, M.; Cheung, H. M. *Langmuir* **1991**, 7, 1, 378.
12. Davis, E. W.; Mukkamala, R.; Cheung, H. M. *Langmuir*, **1998**, 14, 4, 762.
13. Sundell, M. J. *Polymer Preprints*, **1996**, 37, 1, 533.
14. Xue, X.L.; Yin, D. Y.; Ge, X. W.; Ye, Q.; Zhang, Z. C. *Chem. J. Chinese Univ.* **1999**, 20, 3, 478.
15. Pavel, F. M. Macmay, R. A. *Langmuir* **2000**, 16, 8568.

16. Gan, L. M.; Chieng, T.H.; Chew, C. H.; Ng, S. C. *Langmuir* **1994**, 10, 4022.
17. Li, T. D.; Gan, L. M.; Chew, C. H.; Teo, W.K.; Gan, L. H. L*angmuir* **1996**, 12, 5863.
18. Chew, C. H.; Li, T. D.; Gan, L. H.; Quek, C. H.; Gan, L. M. *Langmuir* **1998**, 14, 6068.
19. Challa, V.; Luta, K.; Lopira, S.; Cheung, H. M.; von Meerwall, E. *Langmuir* **2003**, 19, 4154.
20. Eastoe, J.; Towey, T. F.; Robinson, B. H.; Williams, J.; Heenan, R. K. *J. Phys. Chem.* **1993**, 97, 1459.

CHAPTER 2

EXPERIMENTAL

2.1 MATERIALS

Methyl methacrylate (MMA, 99%), ethylene glycol dimethacrylate (EGDMA, 98%), 2-hydroxylethyl methacrylate (HEMA, 97%), acrylamide (AAM, 99+%, electrophoresis grade) were purchased from Aldrich. Prepacked inhibitor remover columns for removing hydro-quinone monomethyl ether (MEHQ) were obtained from Aldrich. All monomers in liquid form were obtained inhibited with MEHQ. Inhibitor MEHQ was removed by passing through an inhibitor remover column before polymerization.

2, 2'-azobisisobutyronitrile (AIBN, 98%), benzoyl peroxide (BPO, 97%), ammonium persulfate (APS, >98%), N,N,N',N'-tetramethylethylenediamine (99.5%), and 2, 2-dimethoxy-2-phenylacetophenone (99%) were purchased from Aldrich and were used without further purification.

Dioctylsulfosuccinate sodium salt (AOT, Aerosol OT, 100%) solid was purchased from Aldrich and from Fisher. 2-(Methacryloyloxy)ethyl

trimethylammonium chloride(MADQUAT) solution, 75 wt% in water, and 2-(acryloyloxy)ethyl trimethylammonium chloride solution, 80 wt% in water were purchased from Aldrich. Solvent ether (99%) was purchased from Aldrich. Ethanol (95%) was purchased from Fisher.

Sulfuric acid was from Dupont. Silver nitrate(99.9%), sodium nitrate(99%) were purchased from Aldrich. Sodium bicarbonate(A.C.S. grade) and ethanol (95%) were purchased from Fisher. AG® MP-50 resin (analytical grade, 100-200 mesh, hydrogen form) and Bio-Rex® 70 Resin (50-100 mesh, Na^+ form) were purchased from BIO-RAD Laboratories, Inc.

Zinc (granular, 99%), (2-Ethylhexyl) hydrogenphosphate (98%), sodium methoxide (97%), and methanol(99.9%), trimethylamine (anhydrous), 11-bromoundecanol (99%), and acryloyl chloride (97%) were purchased from Aldrich and were used as supplied. Dry tetrahydrofuran (THF) was also purchased from Aldrich

Deionized water was used throughout the project.

2.2 METHODS

2.2.1 Preparation of Surfactants

Preparation of (2-methacryloyloxy)ethyl trimethylammonium dioctylsulfosuccinate (MDOS)

MDOS is polymerizable analogue of AOT which is synthesized by liquid-liquid ion-exchange of AOT. [1] MDOS was recovered by evaporating solvent. See Chapter 3 for details.

Preparation of (2-acryloyloxy)ethyl trimethylammonium dioctylsulfosuccinate (ADOS)

ADOS was synthesized using the same method that has been used to synthesize MDOS. ADOS was recovered by evaporating solvent. See Chapter 3 for details.

Preparation of Ag(AOT)

Ag(AOT) was prepared using a two-step ion-exchange method. [2] In the first step, a strong cation exchanger is used to exchange Na^+ of AOT with H^+. In the second step, a weakly acid ion-exchange resin previously put into the Ag^+ form is used to exchange H^+ with Ag^+. Ag(AOT) was recovered by evaporating solvent. See Chapter 3 for details.

Preparation of $Zn(AOT)_2$

Zinc metal is refluxed with the acid form of AOT in 50:50 ethanol solution over night. $Zn(AOT)_2$ was recovered by evaporating solvent. See Chapter 3 for details.

Preparation of Sodium Bis(2-ethylhexyl) Phosphate

Bis(2-ethylhexyl) hydrogen phosphate was dissolved in methanol and titrated with sodium methoxide dissolved in methanol. Sodium bis(2-ethylhexyl) phosphate was recovered by evaporating solvent methanol. [3-5]

Preparation of 11-acryloyloxyundecyltrimethylammonium bromide

A method reported by Gan et al was carefully followed to prepare this polymerizable surfactant. [6] See Chapter 3 for details.

2.2.2 Phase Diagram Mapping

Ternary phase diagrams of water/surfactant/oil have been determined by visual titration of water with surfactant-in-oil solutions in sealed culture tubes or vials with PTFE coated rubber liners at room temperature (22±1°C). Surfactant, oil, and water were mixed thoroughly

either by hand shaking or a Wrist® action shaker or ultrasonicator. The transparency or turbidity of such systems after equilibrium indicates microemulsions and reverse microemulsions are a thermodynamically stable single-phase microemulsion solution or a multi-phase composition, respectively.

To determined L_2 domain, measurements of how much water can be solubilized in a surfactant/oil solution were carried out. Water was added into surfactant/oil solution by Finnpipet, and then the mixture was shaken by hand or was sonicated when needed to see if it forms a clear solution or not until the mixture was turbid after equilibrium. Then direction of titration was switched reversely. Surfactant-oil solution was added into the mixture. The boundary points were determined when the difference between turbid and clear points fell into acceptable uncertainty. Titrations can be done at various concentrations of surfactant in oil up to the solubility of surfactant in oil.

Usually, at high concentration, surfactant/oil solutions are very viscous. It takes a long time for surfactant to dissolve. For example, it takes about one week to dissolve AOT in MMA at 80 wt% and the solution is highly viscous. In such cases, we only map out the L_2 domain up to where we are interested. Figure 2.1 illustrates the path on a ternary phase diagram of water/surfactant/oil system when water is added into surfactant-oil

solution or vice versa. L_1 microemulsion can be mapped out the same way.

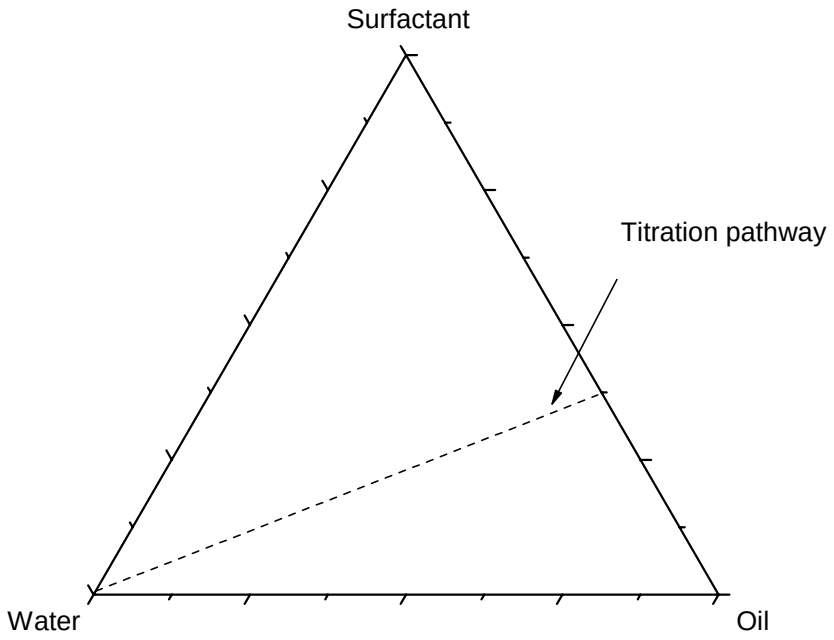

Figure 2.1 Visual titration path along a composition segment having constant surfactant/oil ratio.

It requires very high level of surfactant, often exceeds solubility of surfactant in oil to map out the L_1 corner. And it is very hard to get good resolution using the above path. In the case of the aqueous phase was acrylamide in water solution and AOT/MMA system, 20 wt% aqueous acrylimde solution can take up to 25 wt% of AOT. The working paths that are parallel to the water-oil axis can cover large area of L_1 domain and good resolution. So, L_1 domains have been determined by titration

AOT and acrylamide in water solution with AOT in MMA solution. Paths in this format are parallel to water-oil axis and are chosen to obtained more data in the L_1 corner. Figure 2.2 illustrates the path on a ternary phase diagram of water/surfactant/oil system when AOT-oil solution and AOT-aqueous solution are mixed.

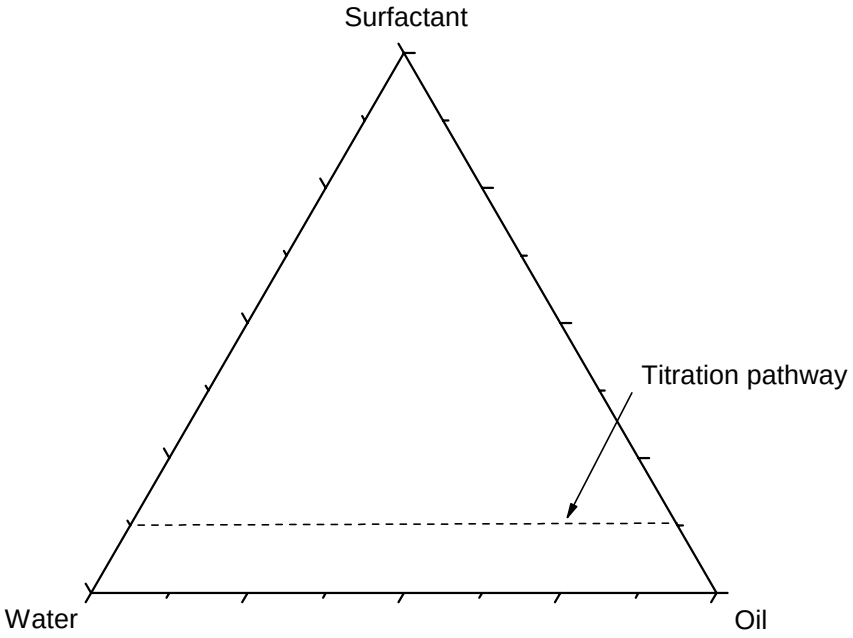

Figure 2.2 Visual titration path along a composition segment having constant surfactant weight fraction.

2.2.3 Conductivity

The conductivity of microemulsions was measured by a Radiometer® CDM 83 digital conductivity meter with an E240 electrode with cell constant $k=0.64cm^{-1}$. The cell constant was calibrated with standard 0.100M KCl at room temperature (22±1°C). Along particular paths (similar to phase boundary visual titration path illustrated in Figure 2.1 and 2.2) in the phase diagram, for examples, we started by adding water into proper amount of surfactant/oil solution in a glass vial with a magnetic stirrer and took readings at each step until the vial was full. Because infinite amount water was needed to achieve 100 wt% of water by adding water into surfactant/oil solution, we started over by adding surfactant/oil solution into proper amount of water solution in a glass vial and took readings at each step and complete the measurement of the whole path.

2.2.4 Polymerizations of Reverse Microemulsion Systems

Most compositions polymerized were in reverse microemulsion domain. Thermal initiators and photo initiators were used. Free radical polymerizations were conducted in sealed 5mm O.D. NMR tubes with 0.015in thick wall, screw-capped PTFE-liner culture tubes, and microscope slides having wells. The reactions were conducted at 50°C and 70°C in water baths, oil baths or ovens. Photo-polymerizations were

carried out at room temperature. Free radical sources, AIBN, BPO and APS were used to initiate polymerization. See Chapter 5 and 6 for details.

2.2.5 Thermogravimetric Analysis

The thermal stability of polymer materials obtained was examined with a thermogravimetric analyzer under air or nitrogen. The instrument used was a TA SDT 2960 (simultaneous DTA-TGA) belonging to Professor Richard Laine at the University of Michigan, Ann Arbor. Samples were heated from room temperature to 600°C at 10°C per minute.

2.2.6 Molecular Weight Analysis

Size Exclusion Chromatography

SEC measurements were conducted by Michele L. Bruck at PRA Laboratories, Inc in Ypsilanti, Michigan. Molecular weight of polymer samples containing AOT were measured by examining dilute samples (0.1% w/w) in THF by size exclusion chromatography using an HP 1050 series HPLC with a HP 1047A RI detector and three Phenogel columns in series as a set for a molecular weight range of 500 to 1,000,000. All samples were dissolved in THF without removing AOT.

Molecular weight analysis of MDOS-MMA copolymers in THF and DMF was unsuccessful by the above SEC method because of incomplete elution of samples with high MDOS content. MDOS-MMA copolymer samples were then sent to Dr. Thomas Mourey at Eastman Kodak Company Research Labs in Rochester, New York.

Molecular weight analysis of MDOS/MMA copolymers were examined in 1,1,1,3,3,3-hexafluoroisopropanol (HFIP)/0.01M tetraethylammonium nitrate. [7] The system has both a viscositry and elastic light scattering detector, which provides absolute molecular weights, radii of gyration, intrinsic viscosity.

2.2.7 Differential Scanning Calorimeter (DSC)

DSC measures temperatures and heat flows associated with thermal transitions in a material. DSC was used to investigate T_g of polymer samples. Heat flow was recorded from 25°C to 200°C at a ramp rate of 20°C per minute.

DSC was also involved in analysis of melting point depression of water that is associated with porosity of polymer samples due to entrapped water. Heat flow was recorded from -40°C to 10°C at a ramp rate of 0.5°C

per minute. The relation for melting point depression of water and radius of pore in nm follows the equation below. [8-10]

$$r(nm) = \frac{-64.67}{\Delta T_m} + 0.57$$

It should be noted that not all of the water present in the samples is seen by melting point depression measurements. Tightly bound water is invisible to the DSC in the temperature range used for our melting point depression measurements. Tightly bound water and the swollen networks containing it undergo transitions at temperatures as low as about 180K. [11, 12]

2.2.8 Scanning Electron Microscopy (SEM)

Selected samples of polymerized microemulsions were kindly analyzed by Professor Renate Hiesgen and Dr Jürgen Kraut of the Physics Department at the Fachhochschule Esslingen, Germany

REFERENCES

1. Eastoe, J.; Towey, T. F.; Robinson, B. H.; Williams, J.; Heenan, R. K. *J. Phys. Chem.* **1993**, 97, 1459.
2. 2 Petit, C.; Lixon, P.; Pileni, M. P. *J. Phys. Chem.* **1993**, 97, 12974.
3. Shioi, A; Harada, M; Tanabe, M J. Phys. Chem. 1995, 99, 4750.
4. Faure, A; Ahlnas, T; Tistlchenko; Chachaty, C. *J. Phys. Chem.* **1987**, 91, 1827.
5. Nakache, E.; Bouloussa, O.; Bourgnet, J.; Lovera, J.; Gregoire, P. *Biochimica et Boiphysica Acta* **1991**, 1074, 413.
6. Li, T. D.; Chew, C. H.; NG, S. C.; Gan, L. M. *JMS-Pure Appl. Chem.* **1995**, A32, 5, 969.
7. Mourey, T. H.; Bryan, T. G. *J. Chromatogr. A.* **2003**, *36*, 2674.
8. Brun, M; Lallenmand, A.; Quinson, J. F.; Eyraud, C. *Thermochim. Acta* **1977**, 21, 59.
9. Quinson, J. F.; Mameri, N; Guihard, L.; Bariou, B. *J. Membr. Sci.* **1991**, 58, 191.
10. Nakao, S. *J. Membr. Sci.* **1994**, 96, 131.
11. Smyyh, G.; Quinn, F. X.; McBrierty, V. J. *Macromolecules* **1988**, 21, 3198.
12. Quinn, F. X.; McBrierty, V. J.; Wilson, A. C.; Friends, G. D. *Macromolecules* **1990**, 23, 4576.

CHAPTER 3

SURFACTANTS

Surfactants play a very important role in microemulsion. Varieties of surfactants used in this project were either purchased or synthesized. Several attempts of synthesizing were successful. Chemical analysis of a few surfactants we prepared did not agree with their proposed structure.

3.1 AOT

Bis(2-ethylhexyl)sulfosuccinate sodium salt, also known as AOT or Aerosol OT, is an anionic surfactant with a double tail. It is capable of stabilizing large amounts of water in organic solvents to form microemulsions without the use of a co-surfactant. [1]

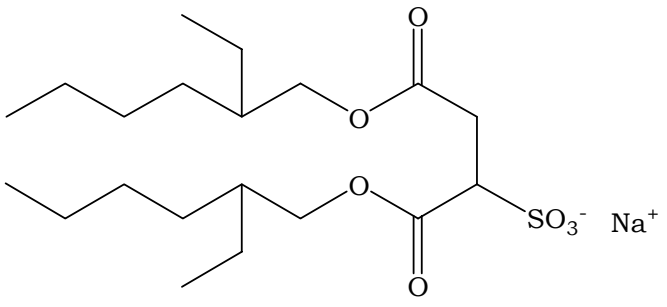

Figure 3.1 double-tail structure of AOT

The two bulky hydrophobic tails coupled with the small head group of AOT favor formation of water-in-oil microemulsions. [1]

AOT dissolves as individual ions in water if its concentration is less than the critical micelle concentration (CMC). Spherical micelles in equilibrium with individual surfactant molecules are formed when concentration is higher larger than the CMC. [2] The presence of aggregated dispersions produces changes in the behavior of the mixture properties as a function of the surfactant concentration. Several techniques, such as conductivity and calorimetric measurements, light scattering, etc. have been used to determine the CMC in these systems. [3] An estimated CMC value for AOT in water obtained through electrical conductivity measurements is 2.2mol/m^3. [2] Hydrocarbon solutions of AOT can take up substantial amount of water and form water-in-oil microemulsions. The size of mono-dispersed and spherical droplets of water is linearly related to the molar ratio of water to AOT. In the following relation, w_0=[$H_2$0]/[AOT] and r_H is the hydrodynamic radius in Angstroms: [4]

$$r_H = 1.75 w_0 + 15$$

In Chapter 4, phase diagrams of AOT/MMA systems with water, aqueous acrylamide will be discussed.

The thermal stability of AOT was characterized by TGA from room temperature to 600°C at a heating rate of 10°C per minute and airflow rate of 60ml per minute. From a weight loss profile of AOT (Figure 3.2), we can see that significant decomposition starts at about 280°C and completes at about 340°C. The weight of remnant is about 14 wt% of AOT which is corresponding to Na content of AOT in the form of Na_2O.

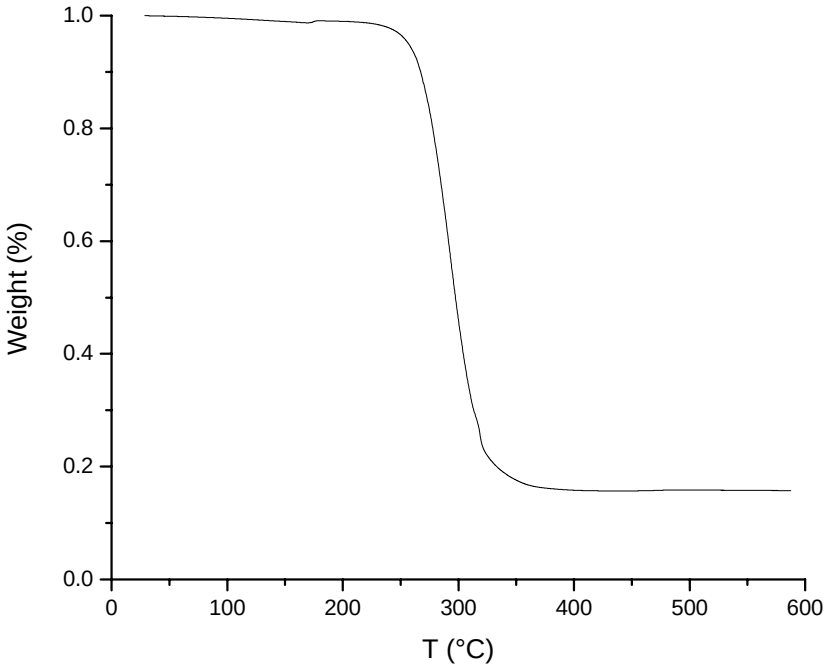

Figure 3.2 TGA of AOT in air

3.2 PREPARATION OF 2-(METHACRYLOYLOXY)ETHYL TRIMETHYLAMMONIUM DIOCYLSULFOSUCCINATE (MDOS)

In order to take advantage of the reverse microemulsion forming capability of AOT anion and polymerizability of 2-(methacryloyloxy)ethyl trimethylammonium chloride(MADQUAT) cation, AOT was ion-exchanged with MADQUAT in a two-phase ether-water system to prepare 2-(methacryloyloxy)ethyl trimethylammonium dioctylsulfosuccinate (MDOS). [5] The nominal structure of MDOS is shown in Figure 3.3.

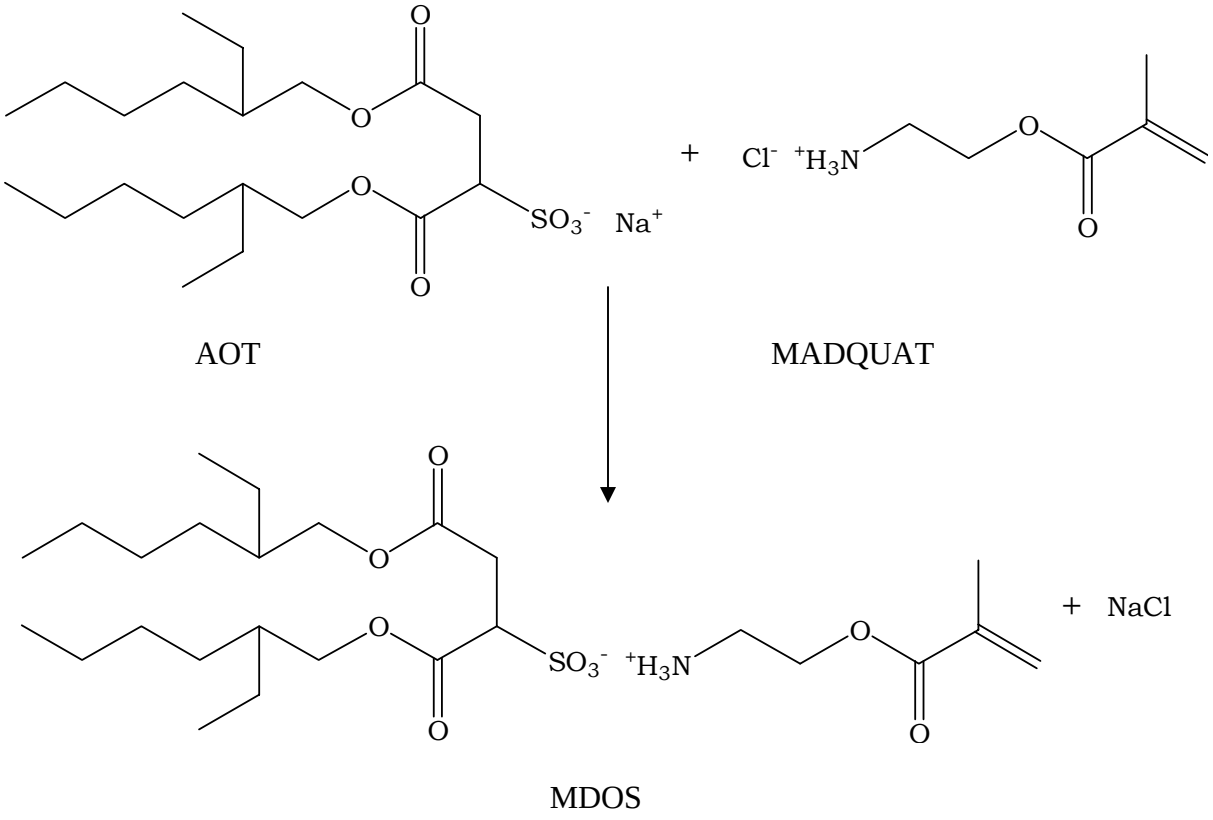

Figure 3.3 Schematic ion-exchange mechanism

The procedure is as follow: approximately 10g of AOT was dissolved in about 200ml ether and was washed with about 6.2g of 75 wt%

MADQUAT diluted to 100ml with deionized water in a 1000ml separatory funnel. Due to the difference of partitioning of each ion in ether and water, we were able to exchange essentially all of the Na^+ of AOT by repeatedly washing and obtain MDOS. Typically the ether phase was washed four times with MADQUAT solution and then with 50ml DI water twice. The final ether phase was separated. The ether was easily removed by evaporating under vacuum in a Ratovapor at 40°C and then was further dried in a vacuum oven at 50°C overnight. The material obtained is a waxy solid. MDOS was also prepared by skipping the DI water washing steps.

MDOS was chemically analyzed by elemental analysis. Samples were analyzed by the CHN lab of the Chemistry Department at the University of Michigan, Ann Arbor. Chemical analysis results indicated elemental composition is consistent with the proposed structure and the products had only trace residual sodium ion content. Theoretical elemental composition of MDOS and experimental results are compared in Table 3.1.

Table 3.1 MDOS elemental analysis results

Sample	%C	%H	%N	%S	%Na	description
Theoretical	58.66	9.34	2.36	5.40	0	Theoretical
MDOS1	58.48	9.84	2.51	5.65	0.20	No water wash
MDOS2	58.58	9.75	2.49	6.06	<0.05	No water wash
MDOS3	58.67	9.82	2.52	5.92	<0.05	Water wash
MDOS4	58.37	9.43	2.44	6.10	0.14	Water wash

Chemical analysis results of MDOS without DI water washing are very close to those with the water washing. It appears that water washing can be skipped without significant effects on MDOS purity.

The phase diagrams of MDOS/MMA systems with various aqueous phases will be discussed in Chapter 4.

Thermal stability of MDOS was also characterized by TGA from room temperature to 600°C at a heating rate of 10°C per minute in air. From the weight loss profile of MDOS (Figure 3.4) we can see that significant

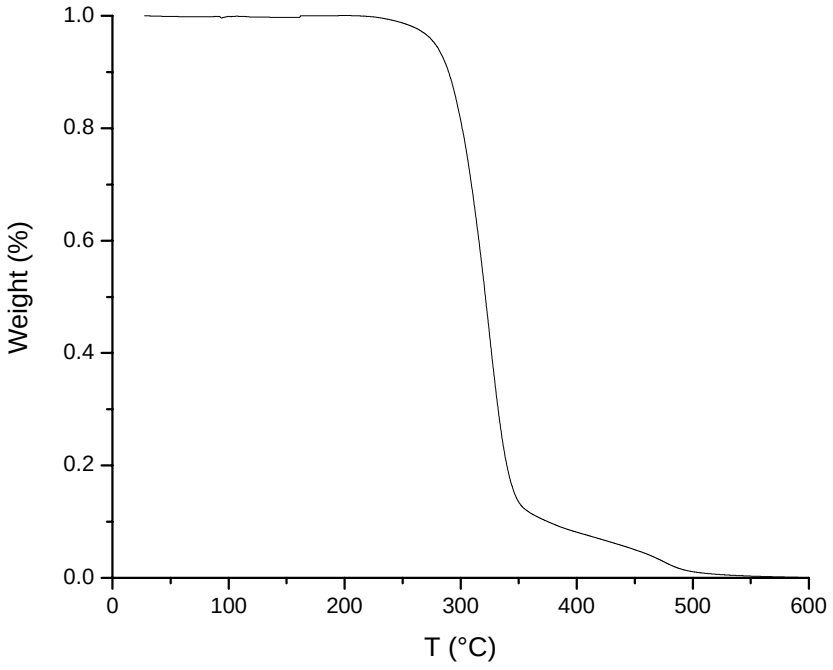

Figure 3.4 TGA of MDOS

decomposition starts at about 280°C and completes at about 550°C. The decomposition is very fast as what is expected for a organic compound. But decomposition deviates to a slower decomposition at about 350°C.

3.3. PREPARATION OF 2-(ACRYLOYLOXY)EHTYL TRIMETHYLAMMONIUM DIOCYLSULFOSUCCINATE (ADOS)

ADOS was prepared with the same method as MDOS was prepared. [5] AOT was ion-exchanged with 2-(acryloyloxy)ethyl trimethylammonium chloride in a two-phase ether-water system by repeatedly washing a solution of AOT in ether (approximately 10g in 200ml ether) with aqueous 2-(acryloyloxy)ethyl trimethylammonium chloride (5.5g 80 wt% diluted to 100ml), followed by washing with distilled water, separating the ether phase, evaporating the ether, and drying the product under vacuum at 50°C. The material obtained was a waxy solid. The nominal structure of the substance, 2-(acryloyloxy)ethyl trimethylammonium bis(2-ethylhexyl)sulfosuccinate, we call ADOS, is illustrated Figure 3.5.

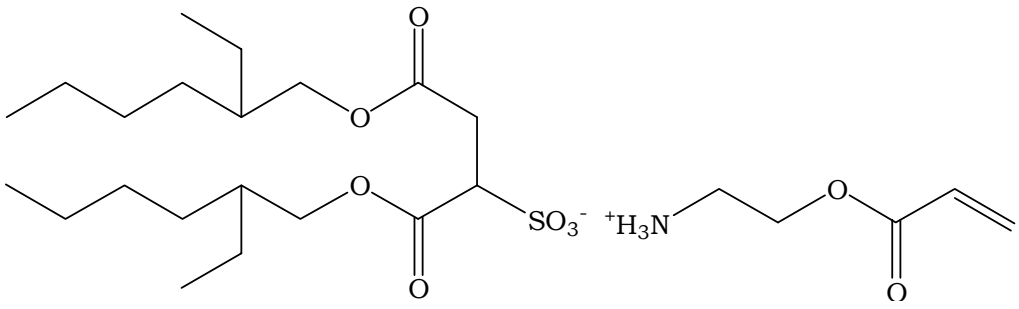

Figure 3.5 Nominal structure of ADOS

ADOS was also chemically analyzed by elemental analysis. Chemical analysis results indicated the product had only trace residual sodium ion content. Theoretical elemental composition of ADOS and experimental results are compared in Table 3.2.

Table 3.2 ADOS elemental analysis results

Sample	%C	%H	%N	%S	%Na	description
Theoretical	58.00	9.21	2.41	5.53	0	Theoretical
ADOS	56.92	9.37	2.52	6.21	0.27	water wash

Chemical composition was consistent with the expected structure and the product had only trace residual sodium ion content.

Our attempts to map out a phase diagram of water/ADOS/MMA failed. We found that our ADOS is not soluble in MMA or in water. It is possible that the ADOS polymerized during the recovery from solvent due to the reactivity of 2-(acryloyloxy)ethyl trimethylammonium group. Further study of this material was temporarily suspended.

3.4 PREPARATION OF Ag(AOT)

Ag(AOT) was prepared by a 2-step ion-exchange method. [6] In the first step, a strong cation exchanger is used to exchange the Na^+ in AOT with

H^+. In the second step, a weakly acid ion-exchange resin previously put in Ag^+ form is used to exchange H^+ with Ag^+.

In the first step, a column containing a strong acid resin, Biorad AG MP-50, 100-200 mesh, in hydrogen form was used to convert Na(AOT) into H(AOT). The column was conditioned with deionized water until pH of water running off the column was around 7.0. Then the column was conditioned with 50 wt% ethanol. Na(AOT) solution of about 0.2M was prepared in a mixed solvent (50 wt% ethanol). The Na(AOT) solution was added slowly to the MP50 column. A pH meter was used to monitor effluent pH. The effluent containing H(AOT) had a in pH range from 0.8~1.2.

In the second step, a column packed with weakly acid resin, Bio-Rex 70, 100-200 mesh in Na^+ was conditioned with a buffer solution of pH 8~9 and then was conditioned with DI water. Buffer solution washing and the water washing were repeated until the pH of water running off the column in water wash was in between 9 and 10 so that Ag^+ would not precipitate while it was being added to the column. A $AgNO_3$ solution of about 0.2M was prepared. Then the Bio-Re 70 column and everything that was used to hold Ag^+ containing substance were carefully wrapped with Aluminum foil in order to prevent Ag^+ from photo-reducing. The above $AgNO_3$ solution was then added to the column slowly. The

procedure was monitored by a combined Ag^+ electrode and a potential meter. When the Ag^+ potential of the solution running off column reached the value of the $AgNO_3$ solution that had been added, the conversion of Bio-Rex 70 resin from Na^+ form to Ag^+ form was completed. The column was then rinsed with DI water until the Ag^+ potential of the water running off column was close enough to DI water. After that, the column was rinsed with about 500ml 50 wt% ethanol and was ready to receive H(AOT) solution.

Bio-Rex 70 resin's selectivity of H^+ is much higher than for Ag^+. H(AOT) from the first step was then slowly added to the column. H^+ was retained and Ag^+ was eluted. Ag(AOT) ran off with the mixed solvent. The ion-exchange procedure was monitored again with the previously mentioned combined Ag^+ electrode and a potential meter.

The collected Ag(AOT) solution was heated up to 98°C in darkness in a Rotavapor to remove the mixed solvent. A light reddish paste was obtained. After further drying the paste in a vacuum oven overnight at 50°C, a light reddish waxy solid was obtained.

Ag (AOT) was chemically analyzed by elemental analysis. Ag was analyzed by titration. Chemical analysis results indicated the elemental composition is not consistent with the expected structure. Compared

with theoretical values, there are a 7.49% short in C, 1.08% short in H, and a 0.78 excess in S, 5.28% excess in Ag. The results suggested partial hydrolysis of ester group of the AOT double tail.

Table 3.3 Ag(AOT) elemental analysis results

Sample	%C	%H	%S	%Ag
Theoretical	45.37	7.04	6.06	20.39
Ag(AOT)	37.88	5.96	6.84	25.67

3.5 PREPARATION OF $Zn(AOT)_2$

Due to the solubility product of $Zn(OH)_2$ is in the order of 10^{-17}, it is not possible to take advantage of ion-exchange method to prepare $Zn(AOT)_2$. The following reaction was proposed to overcome the inconvenience of ion-exchange.

$$2Zn+H(AOT) \rightarrow Zn(AOT)_2+H_2\uparrow$$

Excessive amount of Zn metal was boiled with H(AOT) that was made from the first step ion-exchange in the preparation of Ag(AOT). The reaction lasted about 12 hours. Residue Zn metal was filtered off and solvent was then removed by a Rotavapor. The water bath was heated up to 100°C but not much solvent came out at this temperature. Water was replaced by a silicone oil heating media in order to reach higher

temperature. The system was then heated up to 150ºC. A pasty material was obtained and was further dried in a vacuum oven at 50ºC overnight. The material we obtain appears to be a hard solid.

$Zn(AOT)_2$ was chemically analyzed by elemental analysis. Chemical analysis results indicated an elemental composition not consistent with structure. Compared with theoretical values, the results suggest partial ester hydrolysis. What happened might be that ester group of AOT hydrolyzed and the presence of Zn^{2+} this favors hydrolysis process.

Table 3.4 $Zn(AOT)_2$ elemental analysis results

Sample	%C	%H	%S	%Zn
Theoretical	52.88	8.21	7.06	7.20
$Zn(AOT)_2$	40.15	6.75	8.85	10.1

3.6 PREPARATION OF SODIUM BIS(2-ETHYLETHYLHEXYL) PHOSPHATE

Bis(2-ethylhexyl) hydrogenphosphate and sodium methoxide were dissolved in dry methanol respectively. [7-9] 1.0M solutions of each reagents were prepared in volumic flasks. Sodium bis(2-ethylhexyl) phosphate was prepared by titrating Bis(2-ethylhexyl) hydrogenphosphate with sodium methoxide in methanol media. In this reaction, products were methanol and sodium bis(2-ethylhexyl)

phosphate. The pH was continuously monitored by a pH meter until end point was reached. Methanol was removed by a Rotavapor at 50ºC and then further dried in a vacuum oven at 50ºC. A pasty solid was recovered.

3.7 PREPARATION OF 11-ACRYLOYLOXYUNDECYLTRIMETHYLAMMONIUM BROMIDE [10]

Bromoundecylacrylate (BUA) was first prepared. The bromoundecanol(0.32 mol) and 320 ml THF were mixed in a flask at 0°C under N_2, followed by the addition of 80 mL acryloyl chloride. The reaction system was bubbled with N_2 at room temperature for 2 hours and then left overnight. The unreacted acryloyl chloride and solvent were removed by a rotary evaporator. The yellowish residue was dissolved and washed with saturated sodium hydrogen carbonate solution until the aqueous layer was basic. After evaporation of the ether, a viscous yellowish liquid of BUA was obtained. Acryloyloxyundecyl trimethylammonium bromide (AUMAB) was then prepared. AUMAB was obtained by bubbling trimethylamine gas through BUA dissolved in ether at 0°C. The ether was removed by a Rotavapor and then a vacuum oven at room temperature for three days. The material we obtained was a brownish solid.

AUMBA was chemically analyzed by elemental analysis. Chemical analysis results indicated the elemental composition is not consistent with structure. Our effort on AUMAB was temporarily suspended.

Table 3.5 AUMAB elemental analysis results

Sample	%C	%H	%N
Theoretical	56.04	9.41	3.84
AUTMAB	48.00	9.18	5.95

REFERENCE

1. Russel, A. J.; Komives, C. *Chemtech* **1994**, 1, 26.
2. Acosta, E.; Bisceglia, M; Fernandez, J. C. *Colloids and Surfaces A; Physicochemical and Engineering Aspects* **2000**, 161, 417.
3. Clint, J. H. *Surfactant Aggregation* New York: Blackie & Son, **1992**, Chapter 5.
4. Nicholson, J. D.; Clark, J. H.; *Surfactants in Solution* New York: Plenum Press, **1984**.
5. Eastoe, J.; Towey, T. F.; Robinson, B.H.; Williams, J.; Heenan, R.K. *J. Phys. Chem.* **1993**, 97, 1459.
6. Petit, C.; Lixon, P.; Pileni, M. P. *J. Phys. Chem.* **1993**, 97, 12974.
7. Shioi, A; Harada, M; Tanabe, M J. Phys. Chem. 1995, 99, 4750.
8. Faure, A; Ahlnas, T; Tistlchenko; Chachaty, C. *J. Phys. Chem.* **1987**, 91, 1827.
9. Nakache, E.; Bouloussa, O.; Bourgnet, J.; Lovera, J.; Gregoire, P. *Biochimica et Boiphysica Acta* **1991**, 1074, 413.
10. Li, T. D.; Chew, C. H.; NG, S. C.; Gan, L. M. *JMS-Pure Appl. Chem.* **1995**, A32, 5, 969.

CHAPTER 4

PHASE DIAGRAMS

Surfactants are interface active substances, which stabilize interface between water and oil. Ternary phase diagram is a map for various domains of microstructure. Phase diagrams of varieties of aqueous phase/surfactant/monomer systems are presented in this chapter. Systems containing surfactant AOT or MDOS; aqueous phases of water or aqueous acrylamide; monomer methyl methacrylate (MMA), ethylene glycol dimethacrylate (EGDMA), and 2-hydroxylethyl methacrylate (HEMA) are investigated. L_1 and L_2 boundaries have not been completed due to the viscosity issues.

4.1 PARTIAL PHASE DIAGRAM OF WATER/AOT/MMA SYSTEMS AND CONDUCTIVITY STUDIES

4.1.1 Phase Diagram

The partial ternary phase diagrams of water/surfactant/MMA were determined by visual titration of water into surfactant/MMA solutions in PTFE-liner screw-capped culture tubes. These titrations were conducted

at room temperature 22±1°C. Phase diagram of this system is illustrated in Figure 4.1.

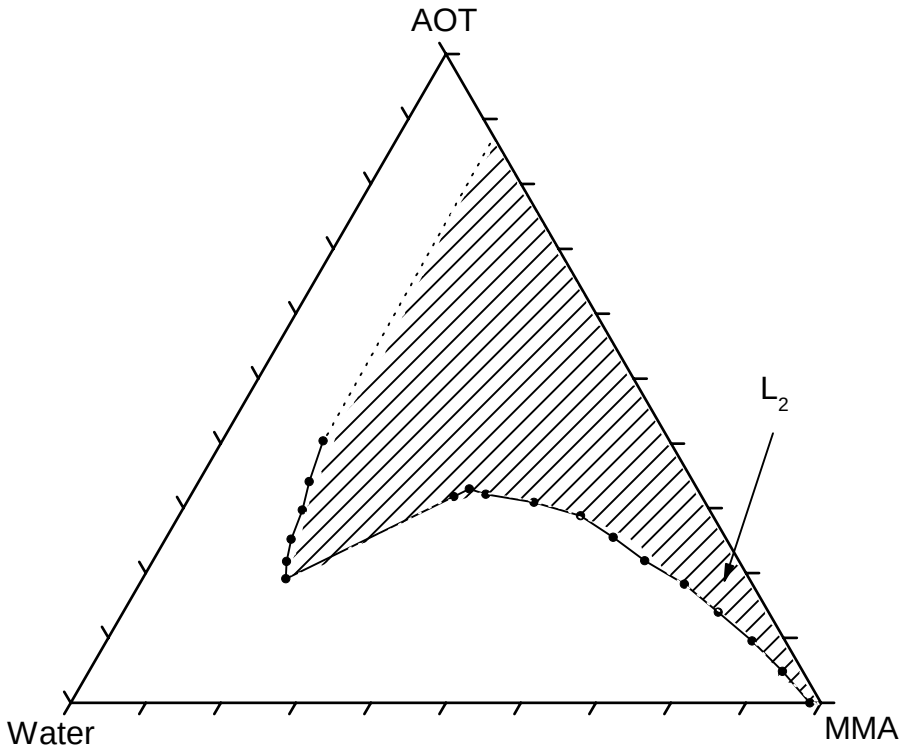

Figure 4.1 Partial single-phase reverse microemulsion domain (L_2) of the water/AOT/MMA system obtained at room temperature (22±1°C). Axes have units of weight fraction. The L_1 domain was also mapped out, but its domain is too small.

The single-phase reverse microemulsion domain (L_2) that is formed by AOT is pretty large. The maximum solubilized water increases gradually from about 2 wt% to 35 wt% as the AOT/MMA ratio is increased up to about an AOT/MMA ratio of 50/50 weight ratio. Above this 50/50 ratio,

the maximum solubilized water increases markedly to about 63 wt% and the decreases with increasing AOT/MMA.

The highest AOT/MMA ratio we studied was 75/25 AOT/MMA. We did not expand our investigation of L_2 boundary further, because the viscosity of the system was too high to allow adequate mixing. So the upper boundary of this domain is approximated in Figure 4.1 by the dotted line running nearly parallel to the water-AOT axis.

The oil-in-water microemulsion single-phase L_1 domain was also mapped. The L_1 domain is rather small on the scale of L_2 domain. As shown in Figure 4.2, the L_1 water corner of the ternary phase diagram is enlarged to show L_1 domain. The maximum solubilized MMA increases from 1.3 wt% with no AOT and reaches its maximum at 8 wt% as the AOT/MMA is increased to a 43/67 weight ratio. Then the boundary turns back markedly to the AOT solubility limit of 1.5 wt% on the water-AOT axis.

Our investigation is consistent with many references that show AOT is capable of stabilizing large amounts of water in organic solvents (Figure 4.3) to form microemulsions without the use of a co-surfactant. [1] But the phase diagram of water/AOT/MMA system we determined does not agree with the result reported by Pavel. [2] In the schematic phase diagram from

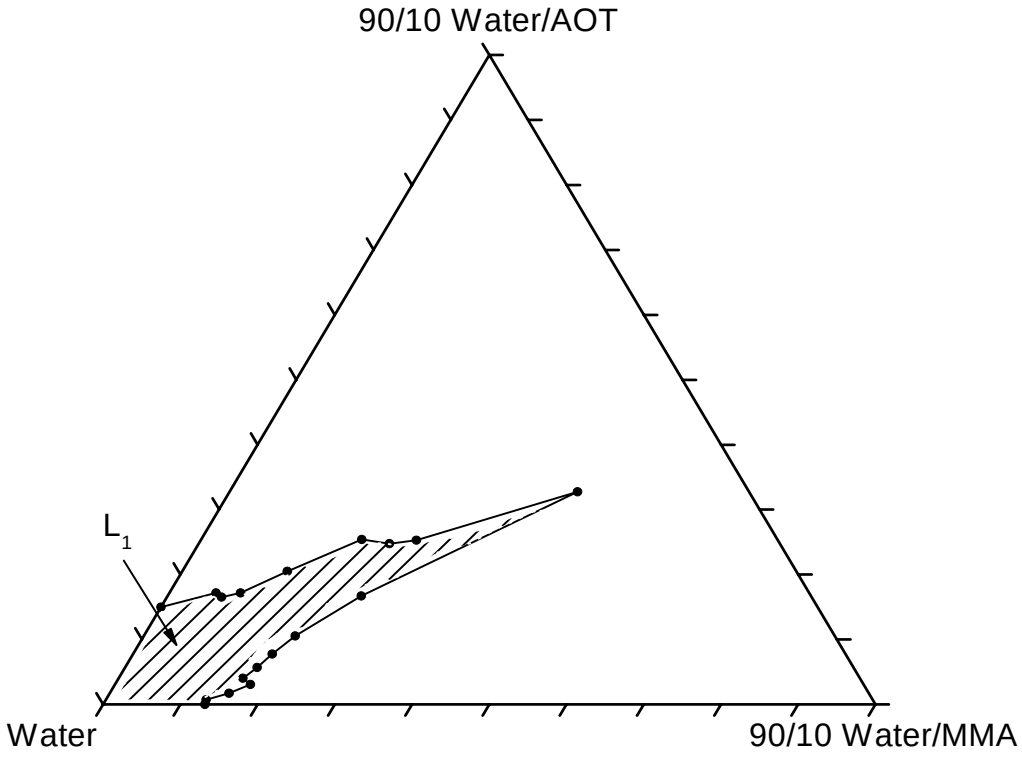

Figure 4.2 Single-phase microemulsion L_1 domain of the water/AOT/MMA system obtained at room temperature (22±1°C). Axes have units of weight fraction. The Water-MMA and Water-AOT axes are scaled to show the 90~100% water corner.

her dissertation (Figure 4.3), it is shown that the water-in-oil microemulsion region expands with increasing AOT and the one phase region in the water corner is very small. And water and MMA corners are simply connected.

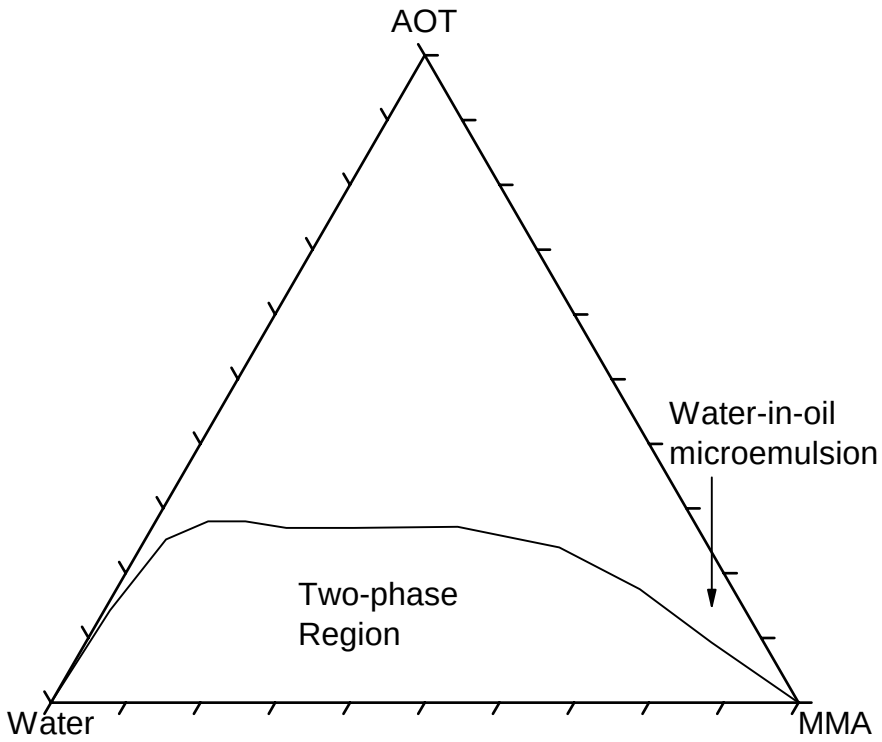

Figure 4.3 Schematic phase diagram of the water/AOT/MMA system. [2]

After a re-examination of the L_2 boundary of this system as a result of the interesting findings in a series of investigations of L_2 boundaries of aqueous acrylamide/AOT/MMA systems (will be discussed later), we found interesting boundary as shown in Figure 4.4 that is more complicated than what are previously shown in Figures 4.1 and 4.3. The multi-phase domain stretches out into L_2 as shown in Figures 4.4. Solubilized water increases as AOT/MMA weight ratio is increased, and

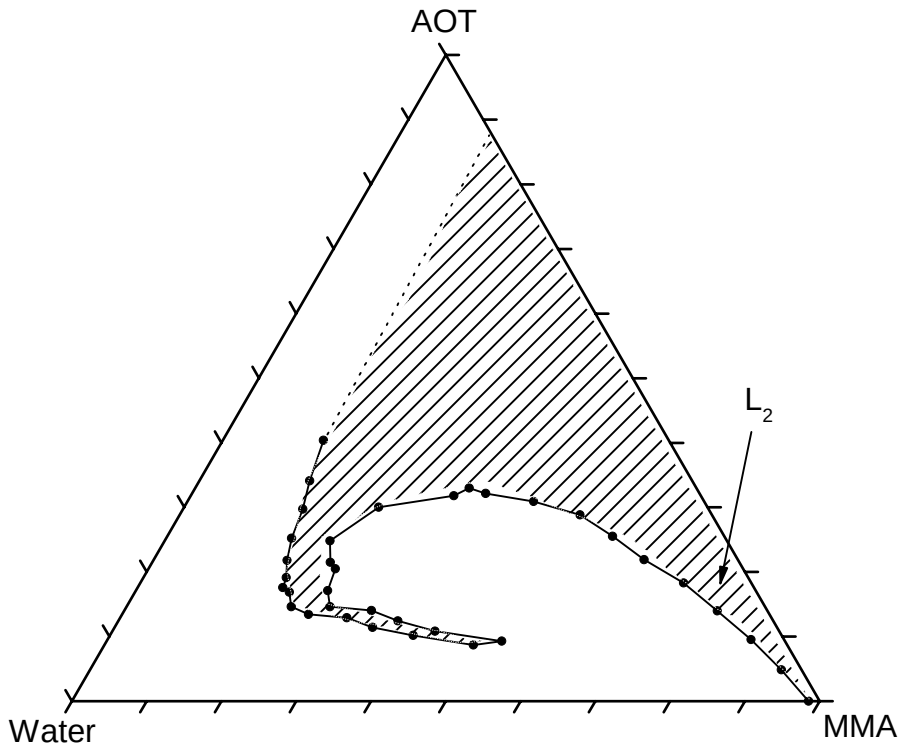

Figure 4.4 Partial single-phase reverse microemulsion domain (L_2) of the water/AOT/MMA system obtained at room temperature (22±1°C). A fish-head-like two-phase domain stretches out into the single-phase region.

then the L_2 turns around to form a fish-head-like domain, and then goes up toward AOT corner. With these new data points of fish-head region, a more detailed partial phase diagram of L_2 was plotted. In the region that we discovered as a single-phase domain, up to 63wt% of water can be solubilized. The microstructure of this domain might be of great interest.

4.1.2 Conductivity

Single phase and optically isotropic microemulsion s are more complex than simple solutions because of the rich zoology of aggregate structures that can exist in such multi-component system. Micro-structural transitions are usually sensible by transport properties that can be monitored by electrical conductivity. [3]

Conductivity studies were conducted at room temperature (22±1°C) for AOT/MMA systems at 30/70, 50/50, 55/45 AOT/MMA ratios in order to examine phase transition in the region where the steep increase of solubilized water occurs. Figure 4.5 shows the loci where conductivity was measured. Two of the paths are above the steep rise and one is below it. The resulting conductivity data are plotted in Figure 4.6.

At the 30/70 AOT/MMA ratio, conductivity increases over one order of magnitude steadily over the range of 0~13% water within the L_2 domain. And then it remains almost constant all the way across the L_2 boundary into the two-phase region as far as 20 wt% of water.

At 50/50 AOT/MMA ratio, conductivity increases over two orders of magnitude over the range of 0~25% water within the L_2 domain. Then it deceases a little bit and stays almost constant over 30~50 wt% water. A

dramatic further increase of conductivity starts at about 50 wt% water within the L_2 domain and extends all the way across the boundary into

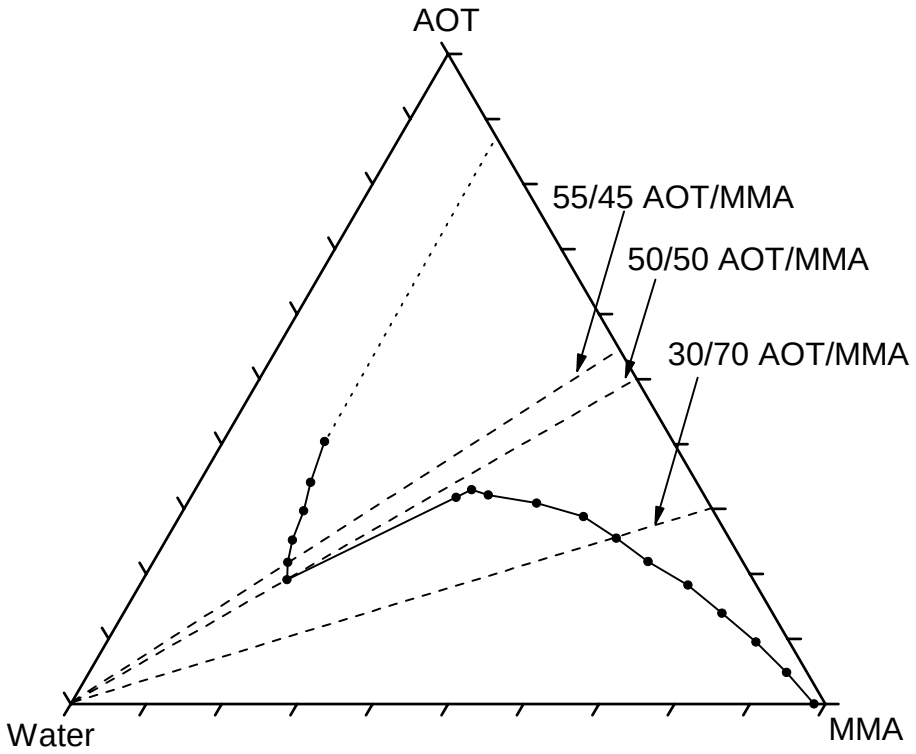

Figure 4.5 Three dashed lines show the paths where conductivity was studied. Two of them are located above 50/50 AOT/MMA ratio in order to investigate the dramatic increase of L_2 domain around 50/50 AOT/MMA.

the multi-phase region.

The conductivity change at the 55/45 AOT/MMA ratio is similar to that of at 50/50 AOT/MMA. Conductivity increases 100 fold over the range of 0~25 wt% water within the L_2 domain. Then it reaches a plateau, almost

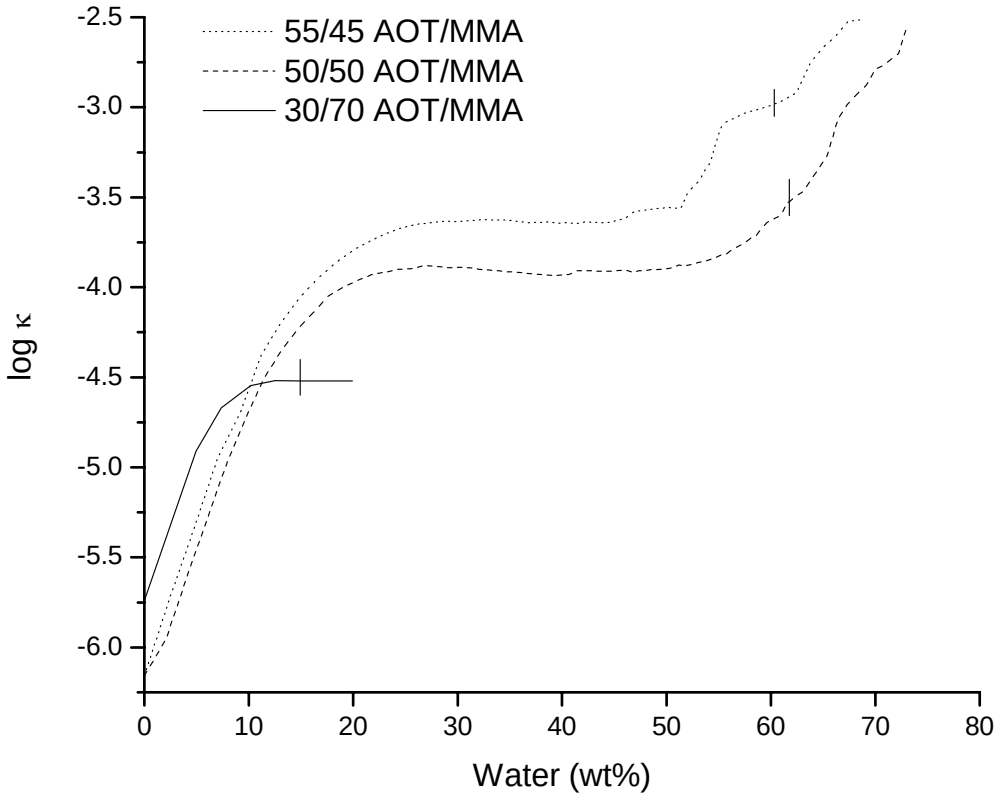

Figure 4.6 Log of conductivity vs. weight fraction of water of AOT/MMA ratio at 30/70, 50/50, and 55/45 obtained at room temperature (22±1°C). Three short vertical ticks on these curves indicate the L_2 boundaries at 14.95, 61.75, and 60.33 wt% water, respectively.

constant over 30~50 wt% water. Again a dramatic increase of

conductivity starts from about 50 wt% water within the L_2 domain and extends into the two-phase region.

It is clearly indicated in Figure 4.6, that the conductivity reaches a plateau over a large segment in the L_2 domain until the L_2 boundary, at 50/50 and 55/45 AOT/MMA ratio where the dramatic increase of L_2 boundary occurs. The transparency and conductivity change suggest continuous phase transitions occur and micro-structures in L_2 domain are not just regular reverse microemulsion. [3]

4.2 PARTIAL PHASE DIAGRAMS OF AQUEOUS ACRYLAMIDE/AOT/MMA SYSTEMS

Partial ternary phase diagrams of 5, 10, and 20 wt% aqueous acrylamide/AOT/MMA systems at room temperature (22±1°C) are illustrated in Figures 4.7, 4.8 and 4.9, respectively. Those dotted lines are the highest compositions verified as belonging to the L_2 domain, which were found along the 75/25, 70/30 and 40/60 AOT/MMA weight ratio segments in 5, 10, 20 wt% aqueous acrylamide system, respectively.

Single-phase reverse microemulsion regions in all three of these diagrams are much larger than in water/AOT/MMA system. The presence

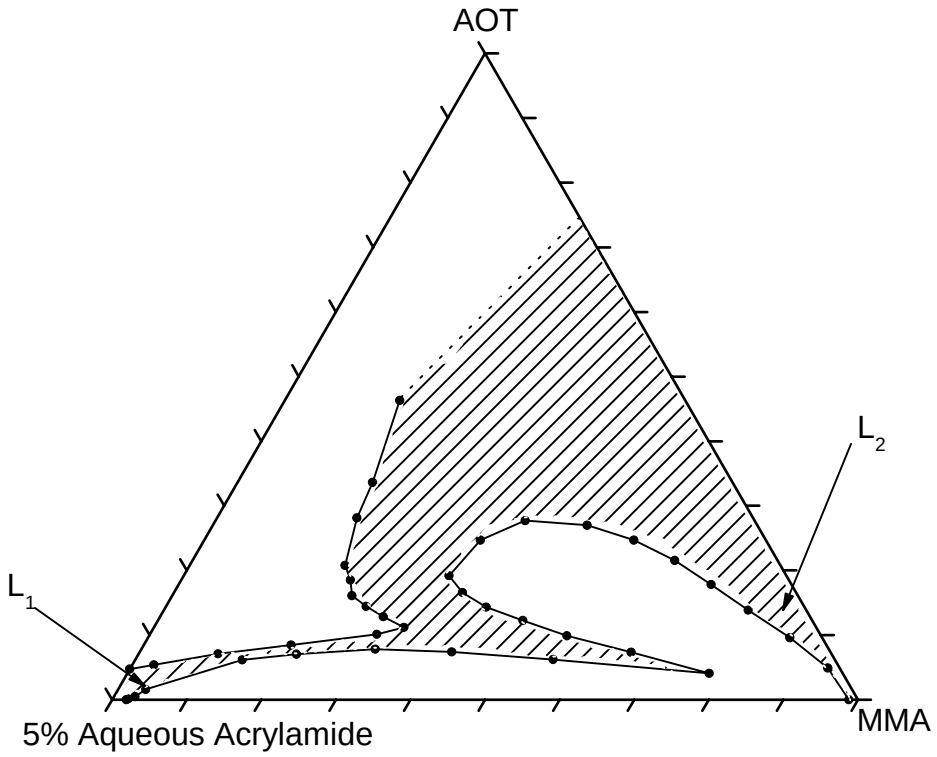

Figure 4.7 Partial single-phase reverse microemulsion domain (L_2) of the 5 wt% aqueous acrylamide/AOT/MMA system obtained at room temperature (22±1°C). Axes have units of weight fraction.

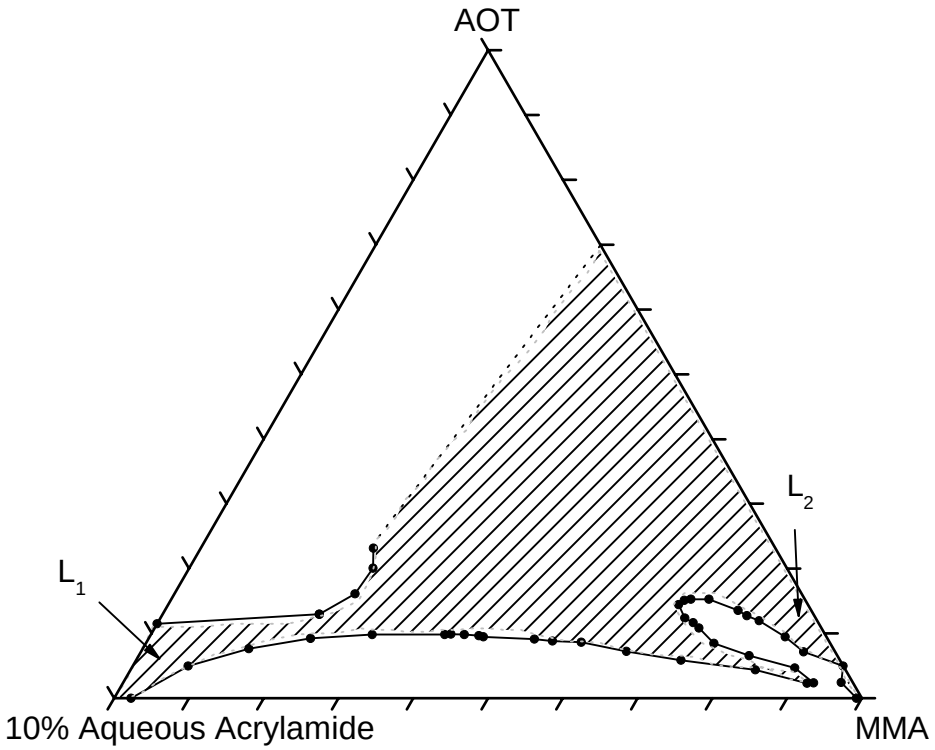

Figure 4.8 Partial single-phase domain of the 10 wt% aqueous acrylamide system obtained at room temperature (22±1°C). Axes have units of weight fraction. The highest AOT compositions verified as belonging to the L_2 domain were found along the 70/30 AOT/MMA weight ratio.

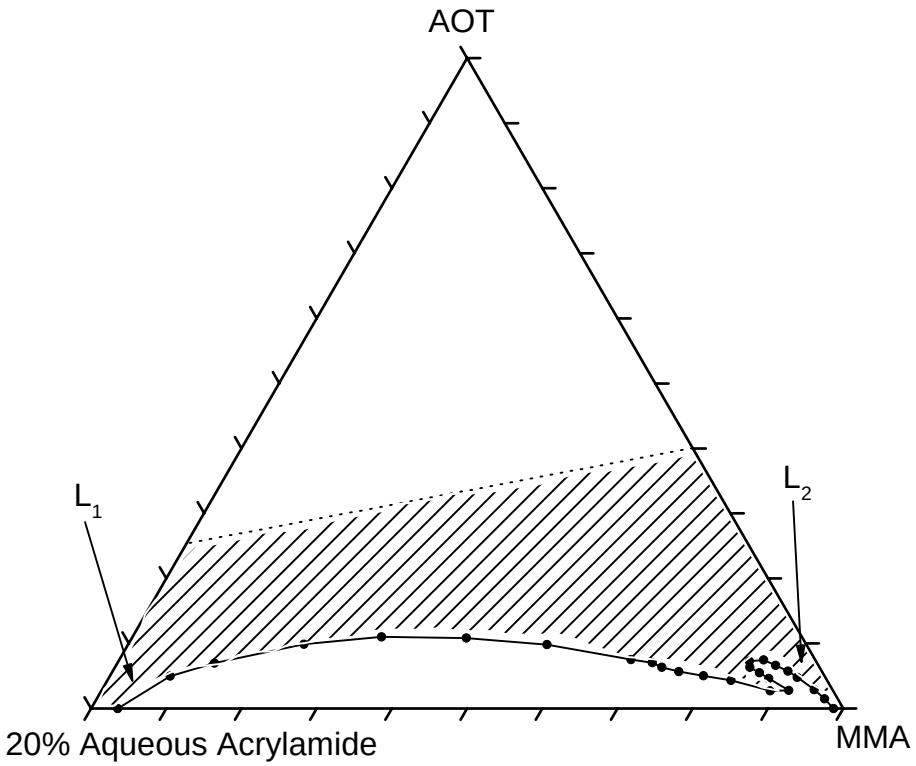

Figure 4.9 Partial single-phase domain of the 20 wt% aqueous acrylamide system at room temperature (22±1°C). Axes have units of weight fraction. The highest AOT compositions verified as belonging to the single-phase domain were found along the dotted line. The upper boundary of single-phase domain has not been determined.

of acrylamide increases the extent of the reverse microemulsion domain. The effects of acrylamide on expanding L_2 domains in reverse water/AOT systems, where the oil phase was toluene has been reported. It is likely that part of acrylamide is located at the interface in between the hydrocarbon chain of AOT. The water-soluble monomer acrylamide plays the role of co-surfactant. [4]

In the L_2 corner of the 5 wt% aqueous acrylamide/AOT/MMA system (Figure 4.7), the two-phase domain extends into single-phase domain and forms fish-head-like boundary which is similar to but smaller than in the water/AOT/MMA system shown in Figure 4.4. The size of two-phase domain and the fish-head region becomes smaller when acrylamide concentration is increased.

It is obvious that the presence of acrylamide increases the extent of the microemulsion domain (L_1), though the L_1 domain is still much smaller than its corresponding L_2 domain. The L_1 domains are much larger than that of water/AOT/MMA system. The L_1 domains of these three systems can be resolved on the scale of L_2.

A very interesting finding is that the presence of acrylamide in the aqueous phase also makes the L_2 and L_1 domains connect by a single-phase channel (Figure 4.8 and 4.9) while in the water/AOT/MMA system

the L_2 and L_1 are separated by turbid multi-phase region. The width of the channel connecting the aqueous and MMA corners increases when acrylamide concentration is increased. At 20 wt% acrylamide, the upper boundary of the single-phase channel is above the dotted line which depicts the highest boundary we have investigated.

The solubility of AOT in aqueous phase increases to about 25 wt% at 20 wt% aqueous acrylamide with increasing acrylamide in aqueous phase as shown in Figure 4.10. The increase of solubility gave us an intuition that acrylamide is also a co-sufactant.

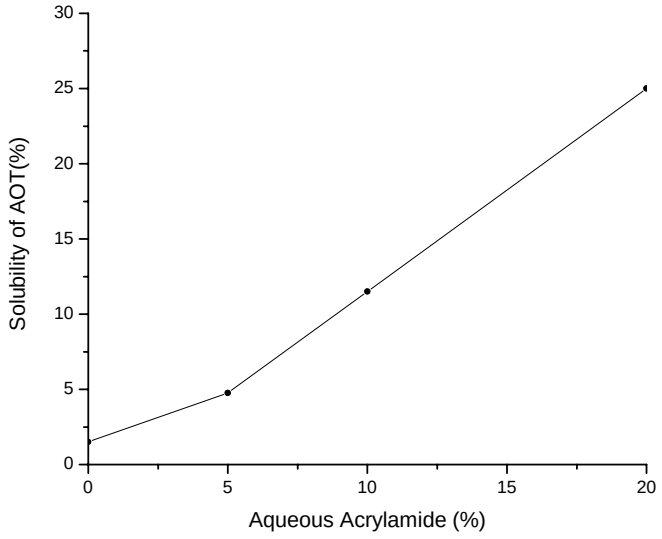

Figure 4.10 Solubility of AOT increases with acrylamide weight fraction.

4.3 PARTIAL PHASE DIAGRAM OF WATER/MDOS/MMA

The ternary phase diagram of water/MDOS/MMA system obtained at room temperature (22±1°C) is illustrated in Figure 4.11.

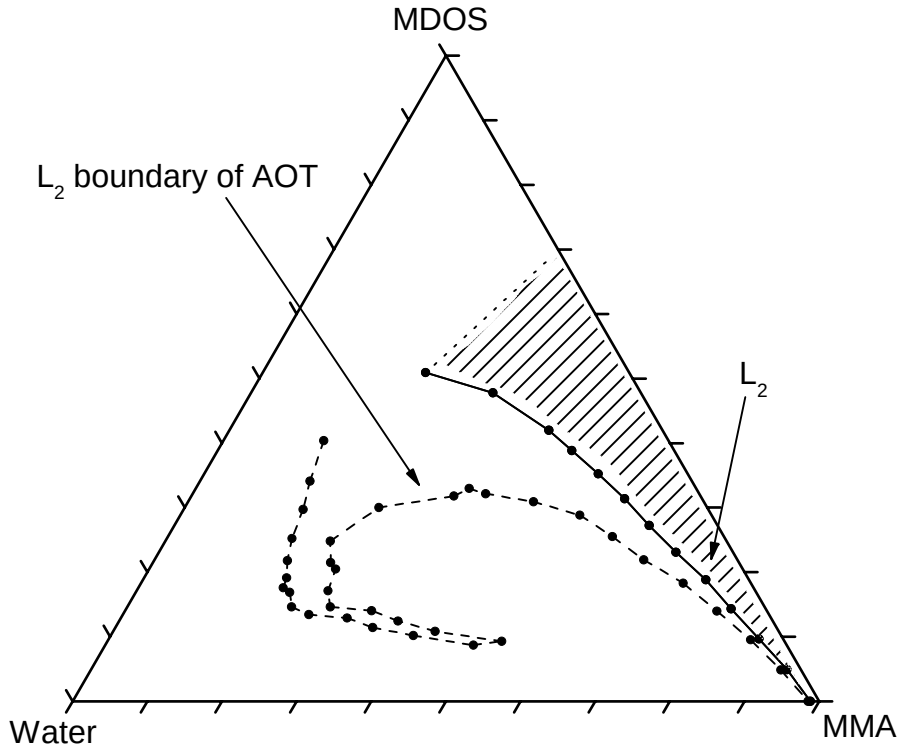

Figure 4.11 Partial phase diagram of reverse microemulsion domain (L_2) of the water/MDOS/MMA system obtained at room temperature (22±1°C). Axes have units of weight fraction.

The area presented as the L_2 domain is fairly large. The highest MDOS compositions verified as belonging to the L2 domain were found along the

70/30 MDOS/MMA line. The size of this L2 domain is about 75% of that obtained with AOT up to 40/60 MDOS/MMA. Above this ratio, the AOT L_2 domain is much larger than the one illustrated here for MDOS. The fish-head domain of the AOT/MMA systems does not present in this water/MDOS/MMA system.

The L_1 domain was also measured. As expected, it is very small as shown in Figure 4.12.

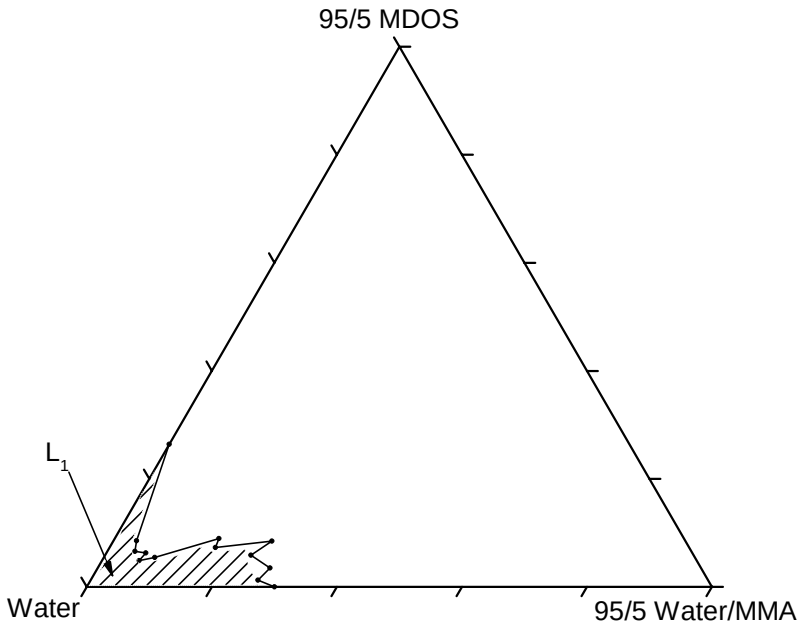

Figure 4.12 Single-phase microemulsion domain (L_1) of the water/MDOS/MMA system obtained at room temperature (22±1°C). Axes have units of weight fraction.

4.4 PHASE DIAGRAMS OF 10 AND 20 wt% AQUEOUS ACRYLAMIDE/MDOS/MMA SYSTEMS

The partial L_2 domain of 10 and 20% aqueous acrylamide/MDOS/MMA systems obtained at room temperature (22±1°C) are illustrated in Figure 4.13.

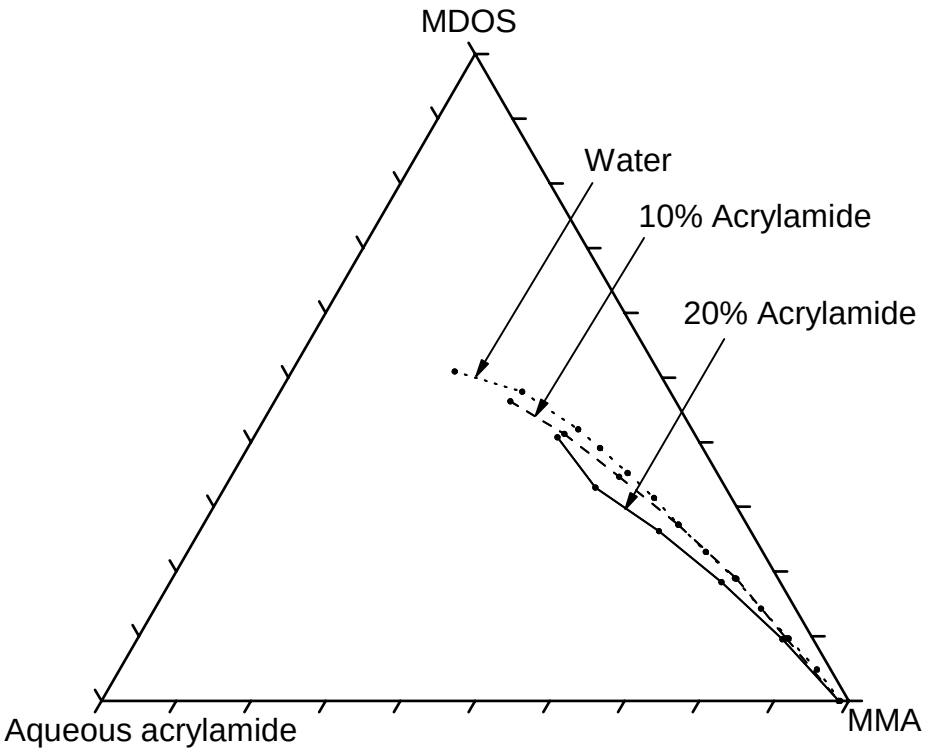

Figure 4.13 Partial phase diagram of the 0, 10, and 20 wt% aqueous acrylamide/MDOS/MMA systems obtained at room temperature (22±1°C). Axes have units of weight fraction.

The area presented as the L_2 domain is fairly large. Due to the extremely high viscosity of the system, the upper region of this domain has not been investigated.

Partial L_1 domains were also measured (Figures 4.14 and 4.15). As expected, they are very small.

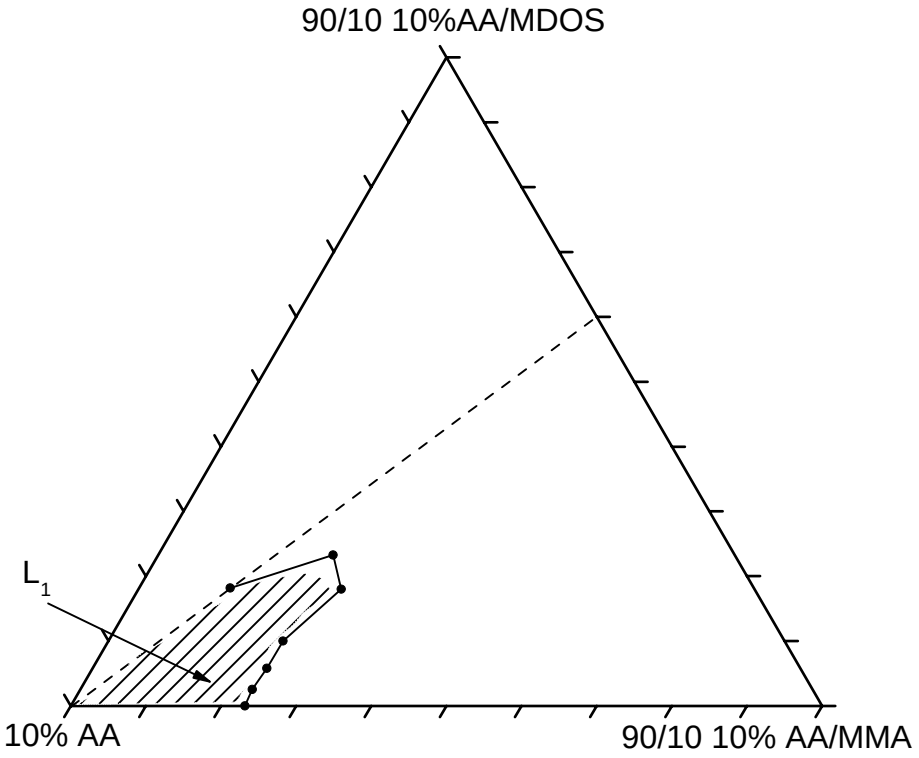

Figure 4.14 Partial phase diagram of the 10 wt% aqueous acrylamide/MDOS/MMA system obtained at room temperature (22±1°C). Axes have units of weight fraction.

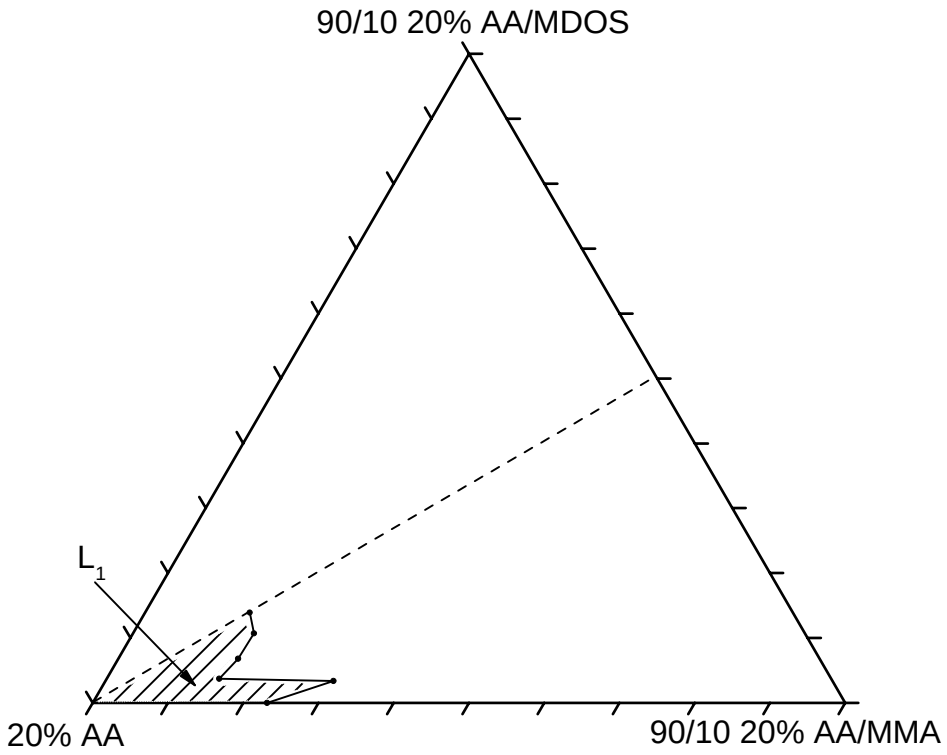

Figure 4.15 Partial phase diagram of the 10 wt% aqueous acrylamide/MDOS/MMA system obtained at room temperature (22±1°C). Axes have units of weight fraction

The increase of the L_2 domain due to acrylamide is not really as large as that of AOT/MMA system. As shown in Figure 4.13, 10 wt% aqueous acrylamide expands the L_2 boundary by about 1 wt%; 20 wt% aqueous acrylamide expands the L_2 boundary by a few percent further.

It is obvious that the presence of acrylamide increases the L_2 domain as well as the L_1 domain. These L_1 domains are very schematic. It appears that the increases of L_1 domains do not correlate with the increase acrylamide concentration.

4.5 PHASE DIAGRAM OF WATER/MDOS/MMA SYSTEMS WITH EGDMA AND/OR HEMA

Polymerization systems often include cross-linking monomer or other monomers to achieve desired properties. Ethylene glycol dimethacrylate (EGDMA), an oil-soluble cross-linking monomer, and hydroxylethyl methacrylate (HEMA), a hydroxyl bearing monomer which might play a role as co-surfactant were introduced into our water/MDOS/MMA system. The phase behavior of such systems was studied.

The ternary phase diagrams the of water/MDOS system with 1:4 EGDMA/MMA and 7:3 MMA/HEMA-5% EGDMA as oil phases obtained at room temperature (22±1°C) are illustrated in Figure 4.16 and Figure 4.17, respectively. The presence of EGDMA and HEMA slightly enlarges the L_2 domain compared with water/MDOS/MMA system. At 20 wt% EGDMA, the L2 domain boundary shifts about 1% left and HEMA pushes the boundary about 2% further.

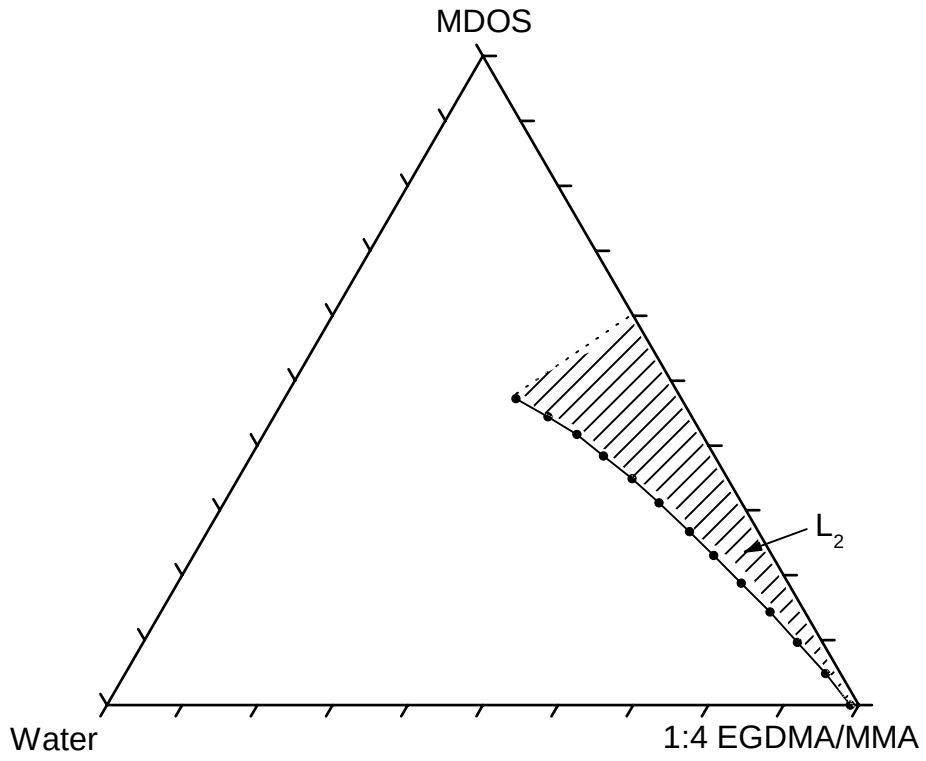

Figure 4.16 Partial phase diagram of the water/MDOS/1:4 EGDMA/MMA system obtained at room temperature (22±1°C). Axes have units of weight fraction. The highest MDOS compositions verified as belonging to the L_2 domain were found along the 60/40 MDOS/1:4 EGDMA/MMA ratio. The L_2 domain is enlarged slightly due to the presence of EGDMA.

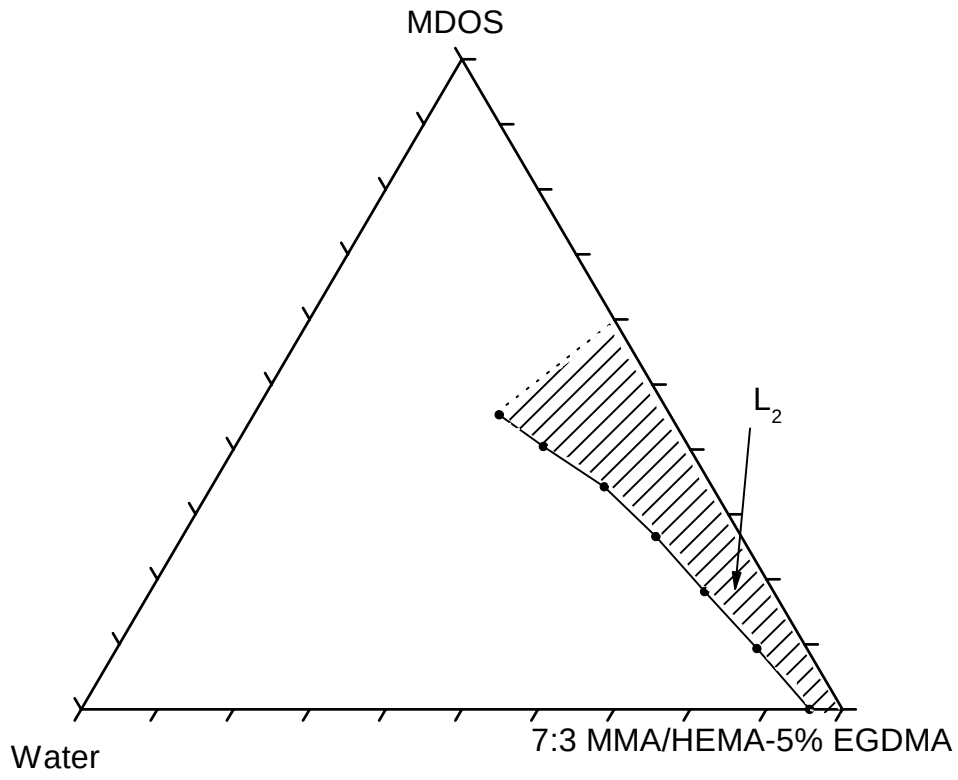

Figure 4.17 Partial phase diagram of the water/MDOS/7:3 MMA:HEMA-5% EGDMA system obtained at room temperature (22±1°C). Axes have units of weight fraction. The highest MDOS compositions verified as belonging to the L_2 domain were found along the 60/40 MDOS/7:3 MMA:HEMA-5% EGDMA ratio. The L_2 domain is further enlarged slightly due to the presence of HEMA.

Partial L_1 domains were also mapped out. It appears that HEMA and EGDMA do not cause expension of L_1 domain. L_2 domains illustrated in Figures 4.18 and 4.19 are very small indeed.

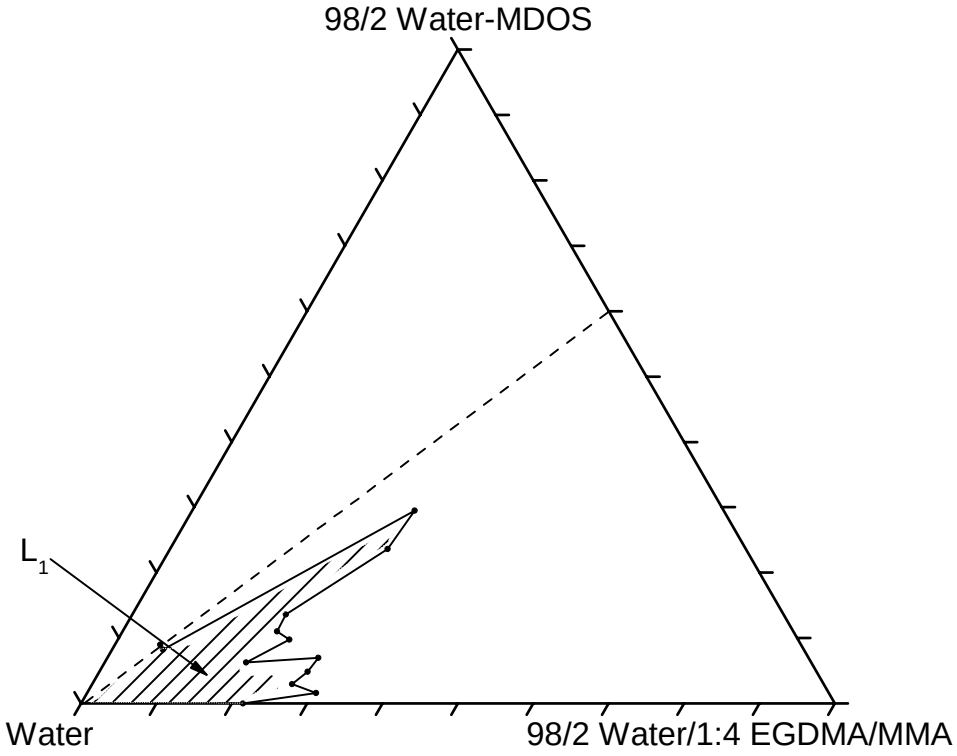

Partial 4.18 Partial phase diagram of the water/MDOS/1:4 EGDMA:MMA system obtained at room temperature (22±1°C). Axes have units of weight fraction. The L_1 domain is very small.

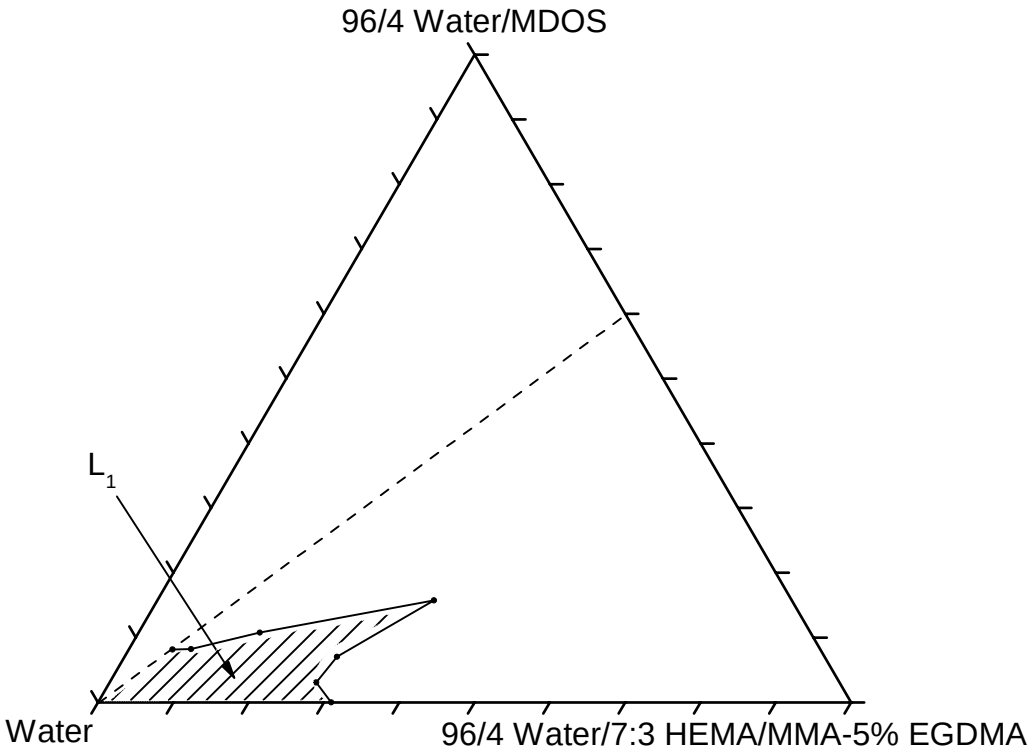

Figure 4.19 Partial phase diagram of the water/MDOS/7/3 MMA/HEMA-5% EGDMA system obtained at room temperature (22±1°C). Axes have units of weight fraction. The L_1 domain is very small.

REFERENCE

1. Russel, A. J.; Komives, C. *Chemtech* **1994**, 1, 26.
2. Pavel, F. M *Polymer Blend and Polymer/Nanoparticle compostites From Microemulsion, Doctorate Dissertation* **2001**.
3. Texter, J. *Colloids and Surfaces A: Physicochemical and Engineering Aspects* **2000**, 167, 115.
4. Chew, C. H.; Gan, L. M. *J. Poly. Sci.* **1995**, 23, 2225.

CHAPTER 5

POLYMERIZATION OF AOT SYSTEMS AND CHARATERIATION

5.1 POLYMERIATIONS

Various compositions within the L_2 domain in the water/AOT/MMA system at 22±1°C were polymerized to capture length of scale of water droplets in PMMA matrix. Polymerizations of aqueous acrylamide/AOT/MMA systems were also studied. The temperature at which polymerizations were conducted was usually higher than room temperature at which phase diagrams were mapped out. The effect of temperature on L_2 boundary investigated for water/MDOS/MMA system. At 70°C, The L_2 domain is slightly larger than that at room temperature. Here we assume that L_2 domains of AOT system also slightly expend at higher temperature.

5.1.1 Polymerization in L_2 Domain of Water/AOT/MMA System

The major purpose of a series of polymerizations in the L_2 domain of water/AOT/MMA system was to investigate conditions that can produce nano-composites of water and PMMA.

A variety of initiator systems were used. Only a few of them were found effective.

Photo initiation: polymerizations were initiated with a UV lamp with or without photo-initiator. Monomer was placed in the well of microscope slide and covered with a piece of thin quartz glass (quartz is transparent to wavelength in UV range while regular glass is not). The slides were exposed to UV radiation for an extend period of time, typically 16 hours. The photoinitiators were used included AIBN at 1%, 2,2-dimethoxy-2-phenylacetophenone at 0.2 wt%, and 4,4'-bis(dimethylamino)-benophenone at 1 wt% of MMA. Neither of the above initiators were effective at room temperature or 40°C.

Redox-initiators: Ammonium persulfate (APS) and N,N,N',N'-tetramethylethylenediamine redox initiation system were used to polymerize water/AOT/MMA reverse microemulsion systems. APS and N,N,N',N'-tetramethylethylenediamine concentrations were 20mmol/L. Monomers were placed in a well-slides or sealed in culture tubes at a

slightly elevated temperature of about 40°C. No solid material was produced after 3 days. This system did not seem to work, either.

Thermal initiators: AIBN is widely used in polymerization. With 0.1, 1, 2% AIBN by weight of MMA, solid materials were successfully produced at 70°C. The PMMA control sample produced was colorless and clear. Another commonly used thermal initiator, benzoyl peroxide was used to polymerize this system at 60°C. Though solid materials were obtained, the products were not colorless.

The compositions marked by crosses in Figure 5.1 were polymerized with AIBN as thermal initiator at 0.1 and 1% of total weight of monomer. The AIBN was dissolved in MMA. AOT/MMA at 30/70 weight ratio was prepared. The weight fraction of water was set at 0, 5 and 10 wt%. Polymerizations were conducted in sealed culture tubes or 5 mm O.D. diameter NMR tubes. These tubes were then immersed in an oil bath at 70C. After about 4~6 hours, the so produced solid rods were recovered from by breaking the tubes.

The solids materials obtained from NMR tubes for 30/70 AOT/MMA with 0, 5, and 10% water are illustrated in Figure 5.2 along with a PMMA control. The photograph was done in order to highlight the translucent

opacity obtained for reverse microemulsion samples and the transparency obtained for the PMMA control.

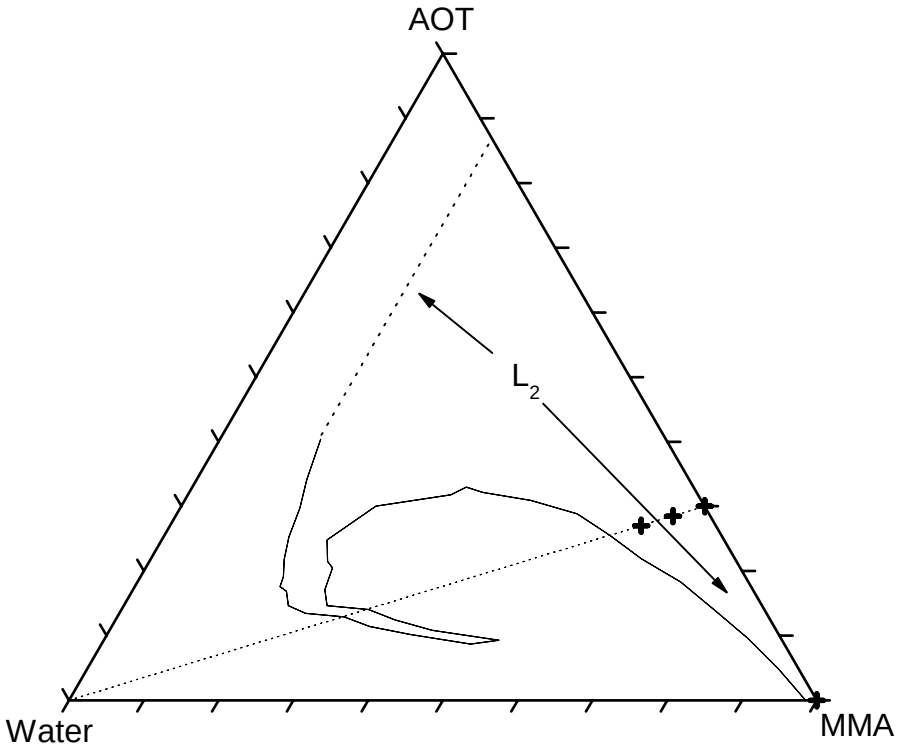

Figure 5.1 Loci of polymerization along the 30/70 AOT/MMA compositional segment within the L_2 domain with 0, 5 and 10 wt% water respectively. AIBN was used as thermal initiator at 70°C. A control sample of PMMA was also produced.

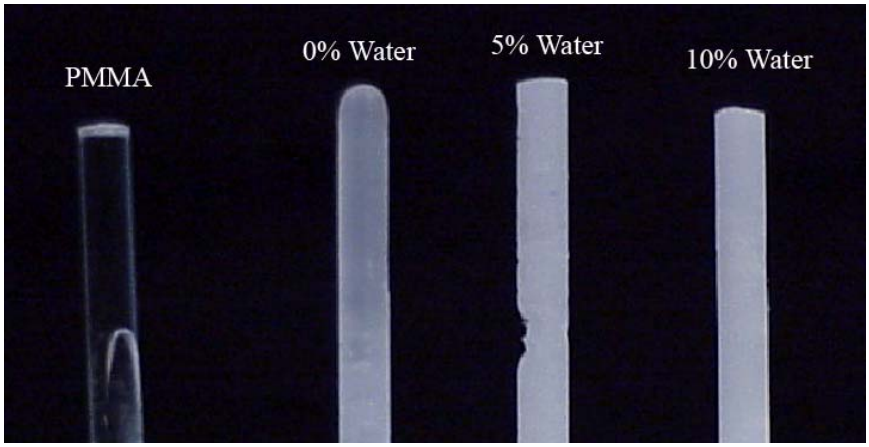

Figure 5.2 Polymerized AOT/PMMA samples. The compositions were formulated at 30/70 AOT/MMA with 0, 5, and 10 wt% water. Turbidity increases with water weight fraction.

Solid materials were also produced at the loci shown in Figure 5.3 under the same conditions. The compositions indicated by the crosses were ±1% in water relative to the L_2 boundary. Although half of the compositions were in L_2 domain before polymerization, the resulting solid rods had similar physical appearances and opacity as the 30/70 AOT/MMA water-containing samples shown in Figure 5.2.

The opacity of the samples is a good evidence for microphase separation during polymerization. All AOT-containing samples were turbid after polymerization. The turbidity and opacity of the water-containing samples was, however, significantly greater than that of the 30/70 AOT/MMA without water illustrated in Figure 5.2. Microphase separation

can be unequivocally assigned as AOT phase separation, and proof from SEM/EDAX data is given in Section 5.2.

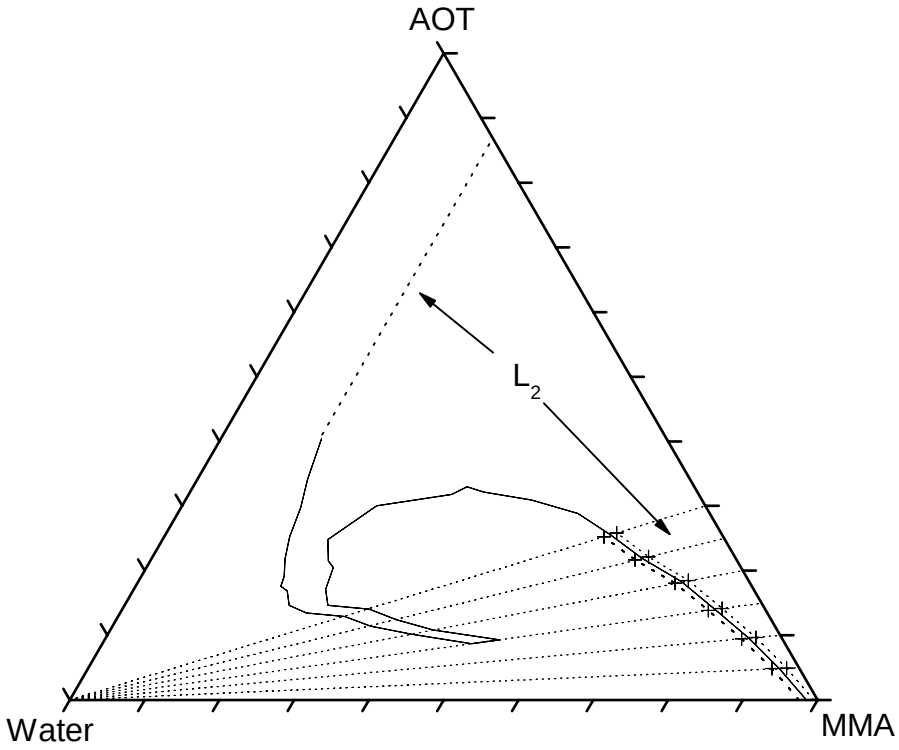

Figure 5.3 Loci of polymerization located in both L_2 and two-phase domains. These polymerizations were conducted at 5% intervals of AOT/MMA from 5 to 30%. The crosses are located ±1% water of the L_2 boundary.

5.1.2 Polymerizations in 20% Aqueous Acaylamide/AOT/MMA System

Compositions within the single phase domain of 20% aqueous acrylamide/AOT/MMA as shown in Figure 5.4 were polymerized.

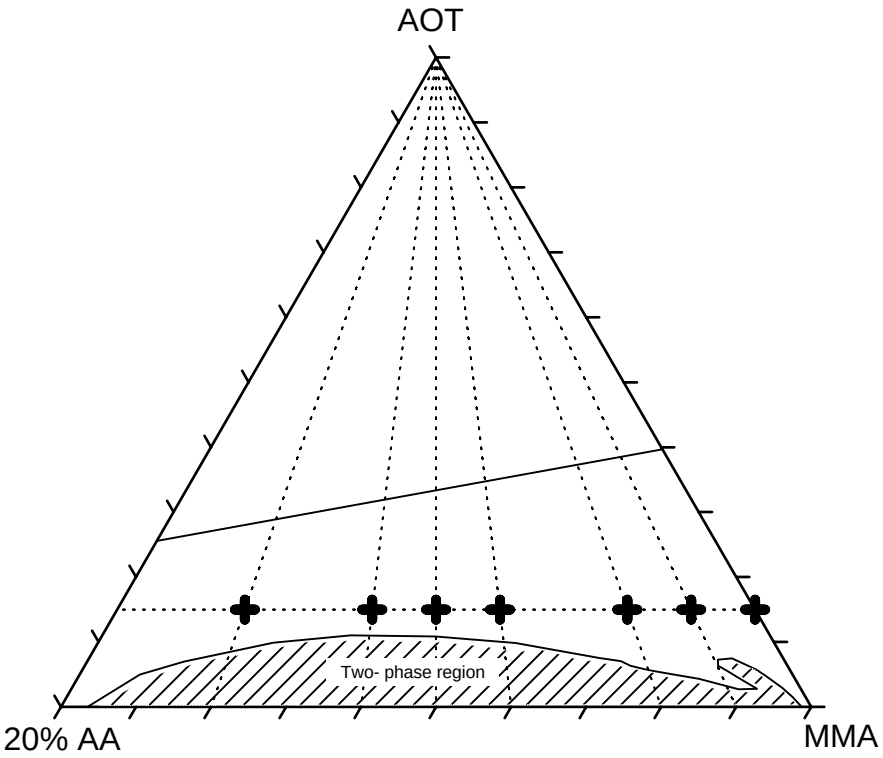

Figure 5.4 Loci of polymerization on 15 wt% AOT path.

AIBN and APS were used as initiators. APS was 0.25% of the weight of aqueous phase and AIBN was 0.1% of the weight of MMA.

Polymerizations were carried out in 5mm O.D. NMR tubes at three different sets of conditions:

(1) Room temperature at about 22±1°C

(2) Room temperature at about 22±1°C for 3 days, followed by heating at 70°C for 4 hours in a oil bath.

(3) Heating at 70°C in an oil bath for 4 hours.

Samples polymerized under condition (1) were half solid half liquid after 3 days of polymerization. Samples polymerized under conditions (2) and (3) were translucent opaque solids. Turbidity or opacity increased with increasing weight fraction of aqueous phase. Rigidity decreased with increasing weight fraction of aqueous phase. Microphase separation occurred in all samples, including those polymerized 15% AOT with no water added.

The samples polymerized under condition set (3) with 20/80, 40/60 and 50/50 aqueous/MMA ratios were not uniform. The bottom portions of those samples were translucent but the top portions are mostly opaque. 60/40 and 80/20 samples were uniform opaque soft materials.

5.2 CHARATERIZATION

5.2.1 Thermostability

As described in Chapter 2, thermal stability was examined using TGA in air from room temperature to 600°C with a 10°C per minute heating rate. TGA results for the samples illustrated in Figure 5.2 are shown in Figure 5.5.

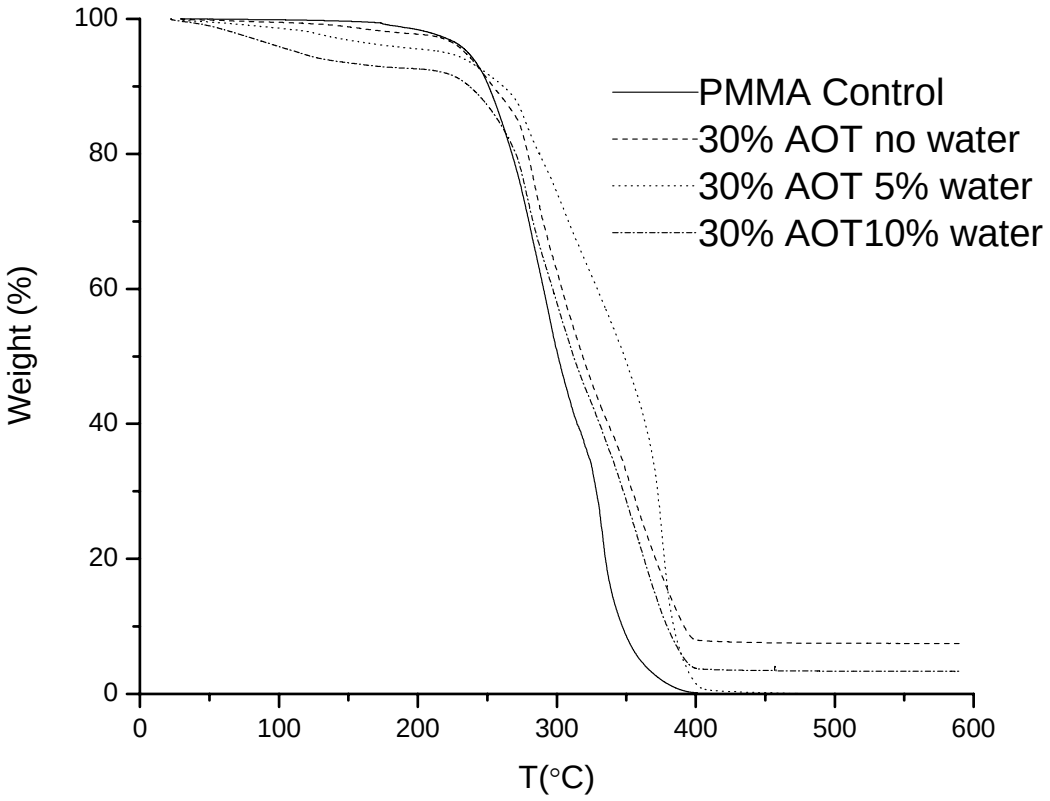

Figure 5.5 TGA weight loss profiles for 30/70 AOT/PMMA samples with 0, 5 and 10 wt% water and a PMMA control.

The PMMA control sample decomposes over the 240-350°C range. The decomposition of all the AOT-containing samples is less than that of PMMA control sample above 270°C. This deviation can be assigned to the presence of AOT, as AOT decomposes over the 270~350°C interval (Figure 3.2).

The overall weight loss of the AOT/PMMA sample without water is slightly greater (0~2%) than that of the PMMA control over 130~220°C interval. The weight loss curves of the two controls samples essentially overlap until the AOT/PMMA sample deviates to a slower decomposition rate at about 250°C. The 5% water AOT/PMMA sample does not begin to loss weight until the temperature reaches about 90°C, and this gradual loss of weight is not complete until about 260°C when decompositions of the polymer sets in. This early weight loss of the 5% water AOT/PMMA sample can be ascribed to release of water at or above the T_g. It is possible that some of the weight loss may be due to un-reacted monomer. However it is unlikely that un-reacted monomer can account for more than 1% weight loss based on the PMMA control and 0% water AOT/PMMA samples. Most of the water diffuses out above 100°C. The 10% water AOT/PMMA sample has similar characteristics to the 5% water sample, except that water loss begins at about 40°C which is just a little bit higher than room temperature. The water release rate of 10% sample is somehow faster than the 5% water sample over the 40~150°C

interval. This phenomenon can be explained by that the porosity of 10% water sample is greater than that of 5% water sample.

Some of the samples generated from polymerizations in 20 wt% aqueous acrylamide/AOT/MMA systems were also characterized by TGA. Figure 5.6 shows the resulting weight loss over room temperature to 600°C interval for samples obtained under condition (3).

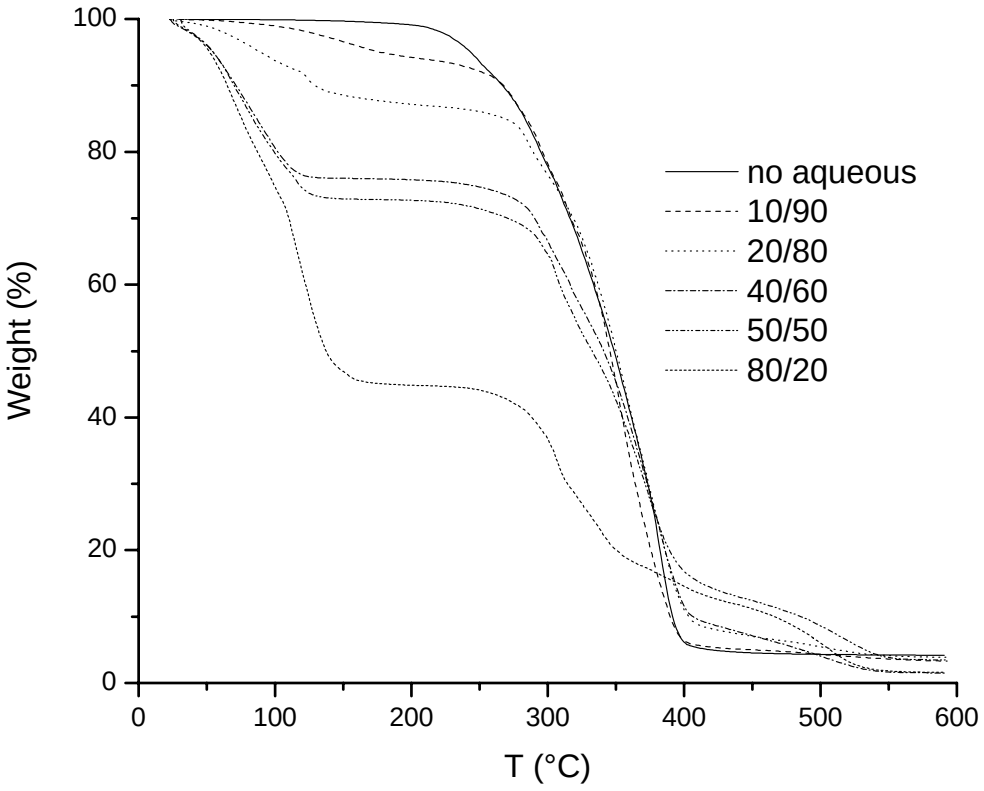

Figure 5.6 TGA weight loss of samples produced at the composition illustrated in Figure 5.4. The ratios correspond to the respective 20% aqueous acrylamide/MMA weight ratios.

The PMMA-AAm samples share similar characteristics with the 30/70 AOT water-containing samples. Water loss begins at about 40°C which is just a little bit higher than room temperature. Most of the water releases over 40~150°C interval, the rest of water diffuses above 150°C. Weight loss before decomposition commences is consistent with corresponding weight fraction of the samples formulation.

5.2.2 Molecular Weight

The 30/70 AOT/PMMA samples containing AOT were analyzed for polystyrene-equivalent molecular weight as described in Chapter 2. The number-average (M_n), weight-average (M_w), and z-average (M_z) molecular weight results and the polydispersity index (*PI*) are summarized in Table 5.1.

Table 5.1 Molecular weight analysis of polymer samples produced by polymerization of 30/70 AOT/MMA containing 0, 5, 10wt% water.

Sample(%water)	AIBN(%)	log M_n	log M_w	log M_z	PI
0%	.0.1	5.79	6.31	6.53	3.33
5%	0.1	5.73	6.32	6.55	3.88
10%	0.1	5.78	6.32	6.54	3.49
PMMA control	1	5.16	5.73	6.12	3.65
0%	1	5.19	5.86	6.19	4.65
5%	1	5.06	5.75	6.10	4.81
10%	1	5.14	5.84	6.17	4.99

The level of initiator has a great impact on molecular weight and polydispersity. The ten-fold increase of AIBN resulted in an approximately 70% decrease of M_w, 76% decrease of M_n, and 60% drop of M_z. The PI increases about 33% with a ten-fold increase of AIBN.

The surfactant AOT and microemulsion seem to have an effect on polydispersity. For the samples with 1% AIBN, the PI is about 30% greater than for the PMMA control.

5.2.3 Glass Transition Temperature

T_g, glass transition temperature, was measured for the PMMA control and 30/70 AOT/PMMA samples. For the PMMA control, the ten-fold increase of initiator AIBN caused the T_g to decrease from 105°C to 103°C For the AOT/PMMA samples, the T_g decreased 7°C from 100°C to 93°C as initiator was increased from 0.1% to 1.0%. AT the same level of AIBN, the AOT/PMMA samples had a lower T_g than the respective PMMA control.

5.2.4 Thermoporosity Analyses by DSC

Some of the AOT samples were analyzed for nano-porosity as described in Chapter 2. [1-3] All of the 30/70 AOT/MMA samples were scanned over

40~10°C interval at 0.5°C per minute heating rate. For 0 and 5% water AOT/PMMA samples, no freezable water was observed. In the case of 10% water sample, approximately 10% of the total water is freezable, but highly perturbed relative to bulk water and this freezable water exhibits a -11.75°C melting point depression (Figure 5.7), which corresponds to a 12nm diameter pore size.

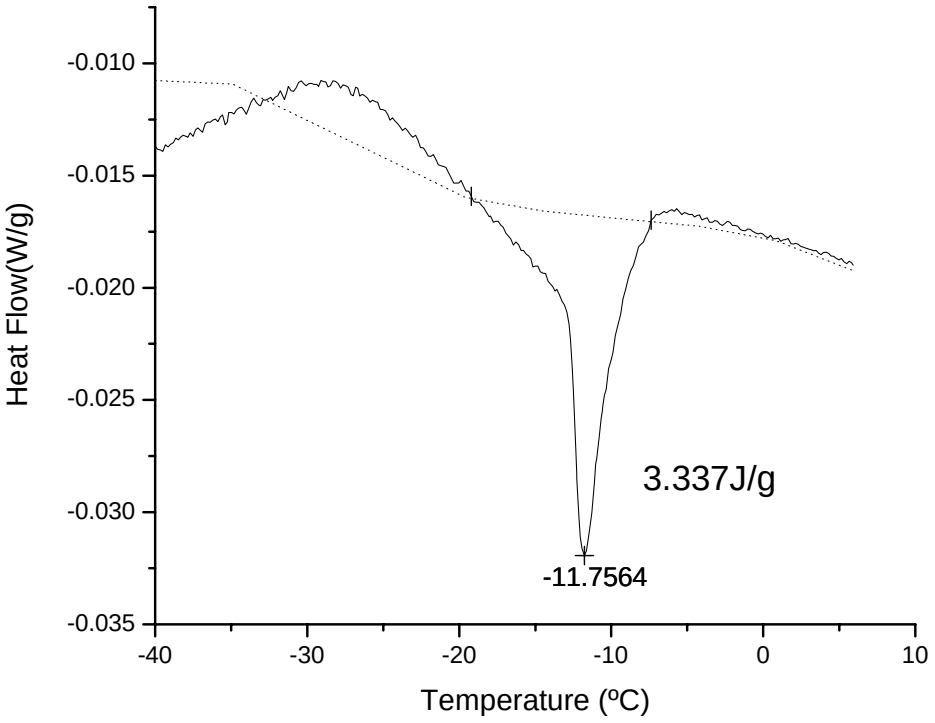

Figure 5.7 DSC data showing -11.75°C melting point depression for 10% water 30/70 AOT/PMMA sample.

This finding, along with the TGA data, indicate that water in the 5% water 30/70 AOT/MMA sample does not contain any freezable water. It

suggests that the water is tightly bound to the surfactant. This water starts going out the samples at about 90°C which is lower than but close to the T_g. In the 10% water sample, about 10% of the water is freezable. It suggests that the sample is somewhat nano-porous with some water released well below the T_g.

The samples produced from the 20% aqueous acrylamide/AOT/MMA system, as illustrated in Figure 5.3 were also analyzed for freezable water. The resulting data are plotted in Figures 5.8~5.15. The corresponding pore sizes are summarized in Table 5.2

Table 5.2 Melting point depression data and porosity analyses for 15% AOT samples illustrated in Figure 5.3

DSC Figure	Aqueous/MMA (w/w)	Peak #	Melting Point Drepression(°C)	Pore size (nm)
5.7	20/80 bottom	0	no freezable water	
5.8	20/80 top	1	-11.58	12.31
		2	-7.54	18.29
5.9	40/60 bottom	1	-11.64	12.25
		2	-7.54	18.29
		3	-1.62	80.98
5.10	40/60 top	1	-11.78	12.12
		2	-7.76	17.81
		3	-1.06	123.16
5.11	50/50 bottom	1	-11.67	12.22
		2	-7.72	17.89
		3	-1.18	110.75
5.12	50/50 top	1	-11.48	12.41
		2	-7.59	18.18
		3	-0.69	188.59
5.13	60/40	1	-11.48	12.41
		2	-7.45	18.50
		3	-0.73	178.32
5.14	80/20	1	-11.23	12.66
		2	-7.4	18.62
		3	-0.72	180.78

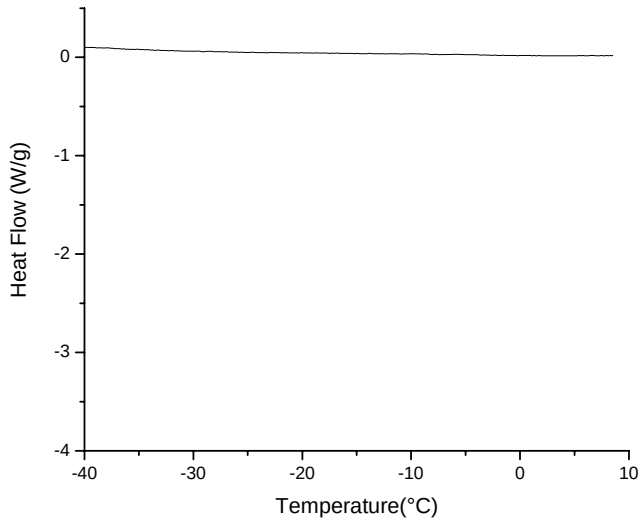

Figure 5.8 Thermoporosity analysis for bottom part of 15% AOT 20/80 aqueous phase/MMA sample. No freezable can be observed from the heat flow curve.

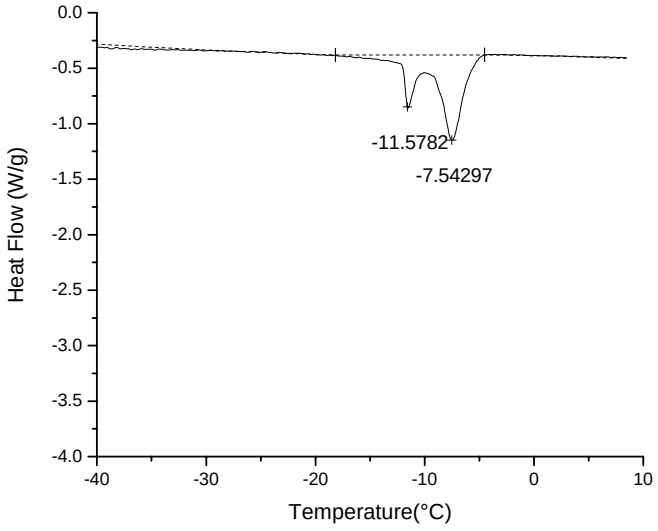

Figure 5.9 Thermoporosity analysis for top part of 15% AOT 20/80 aqueous phase/MMA sample. There are two species of freezable water with depressed melting points.

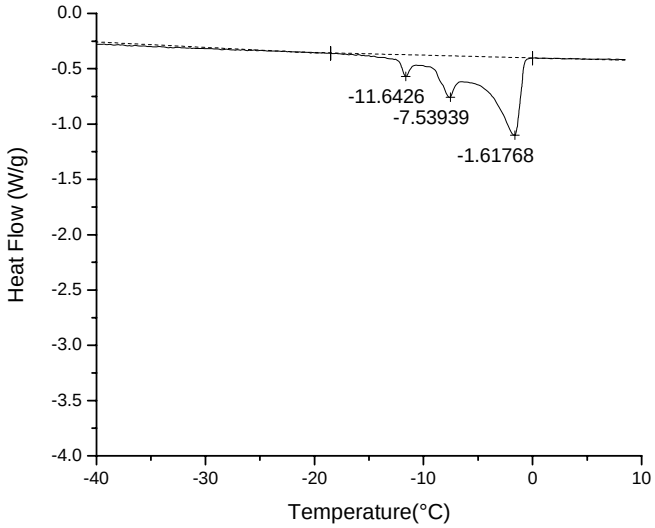

Figure 5.10 Thermoporosity analysis for bottom part of 15% AOT 40/60 aqueous phase/MMA sample. There are three species of freezable water with depressed melting points. The water with a melting point at -1.62ºC is essentially bulk water containing polyacrylamide.

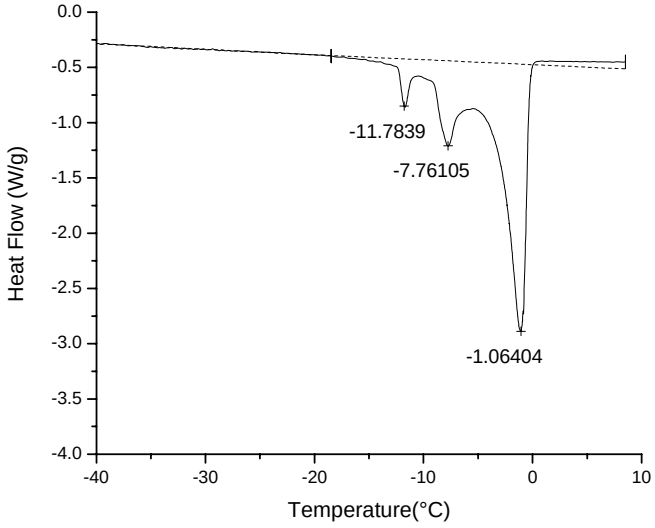

Figure 5.11 Thermoporosity analysis for top part of 15% AOT 40/60 aqueous phase/MMA sample. There are three species of freezable water with depressed melting points. The water with a melting point at -1.06ºC is essentially bulk water containing polyacrylamide.

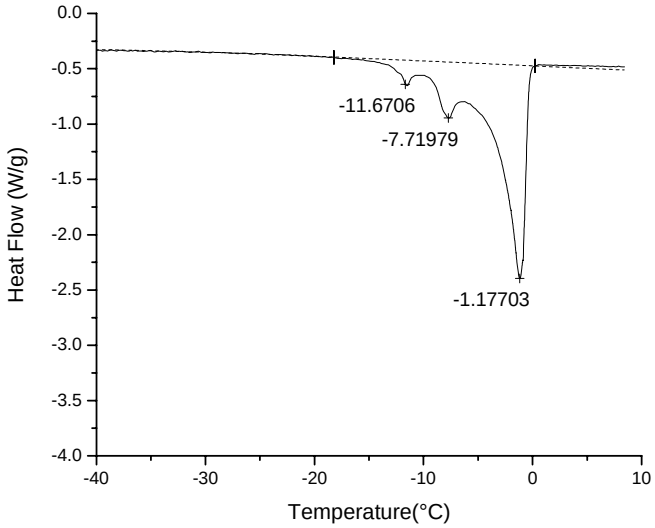

Figure 5.12 Thermoporosity analysis for bottom part of 15% AOT 50/50 aqueous phase/MMA sample. There are three species of freezable water with depressed melting points. The water with a melting point at -1.18ºC is essentially bulk water containing polyacrylamide

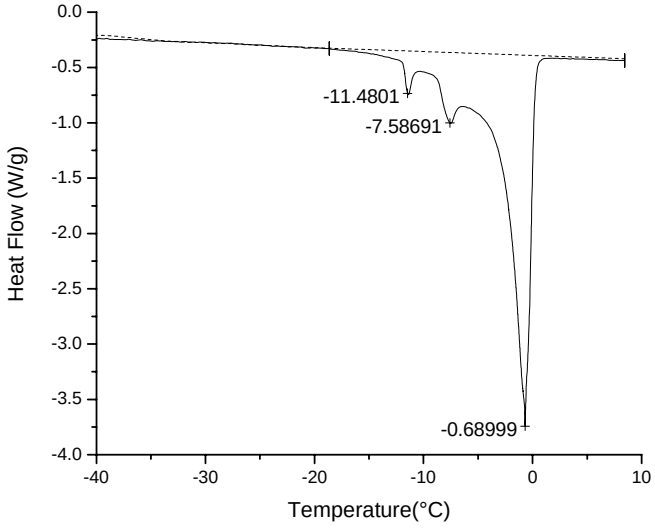

Figure 5.13 Thermoporosity analysis for top part of 15% AOT 50/50 aqueous phase/MMA sample. There are three species of freezable water with depressed melting points. The water with a melting point at -0.69ºC is essentially bulk water containing polyacrylamide

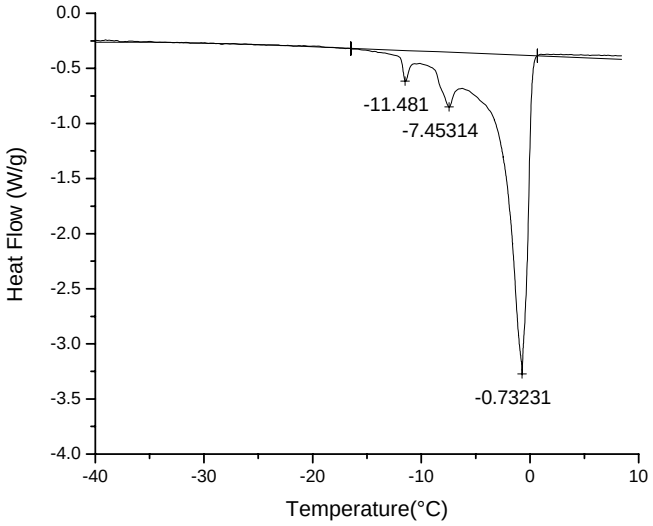

Figure 5.14 Thermoporosity analysis for 15% AOT 60/40 aqueous phase/MMA sample. There are three species of freezable water with depressed melting points. The water with a melting point at -0.73°C is essentially bulk water containing polyacrylamide

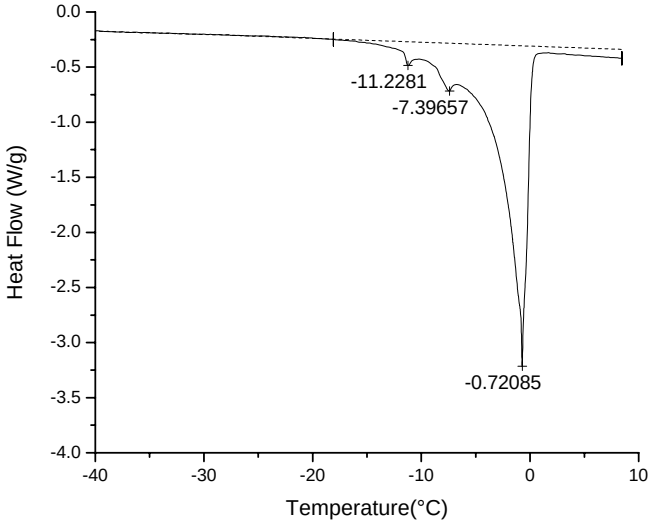

Figure 5.15 Thermoporosity analysis for 15% AOT 80/20 aqueous phase/MMA sample. There are three species of freezable water with depressed melting points. The water with a melting point at -0.72°C is essentially bulk water containing polyacrylamide

The samples with 20/80, 40/60 and 50/50 aqueous/MMA ratio were not uniform. The bottom portions of those samples were translucent, but the top portions were mostly opaque. The 60/40 and 80/20 samples were uniformly opaque and soft materials. The properties of the water in these samples are somewhat different from that in the 10% water 30/70 sample. The species of water with depressed melting points suggests the presence of nano-pores with pore sizes of about 12 nm and 18 nm. A slight depression of melting point can be observed in the 40/60, 50/50, and 60/40 samples suggests the presence of macro-pores in which water behaves more like bulk water. This finding is consistent with the TGA analysis of these samples, where the water in these samples releases well below boiling point of water.

5.2.5 SEM Imaging

The samples produced from 20% aqueous acrylamide/AOT/MMA system as illustrated in Figure 5.3 were also investigated by SEM imaging for porosity.

SEM examination of a Pt/Pd shadowed fracture surface of the 15% AOT 0% water sample (Figure 5.16) revealed a topography exhibiting a very smooth fracture surface, such as that annotated 2-2 in Figure 5.16, and hemispherical depressions having a rough surface texture.

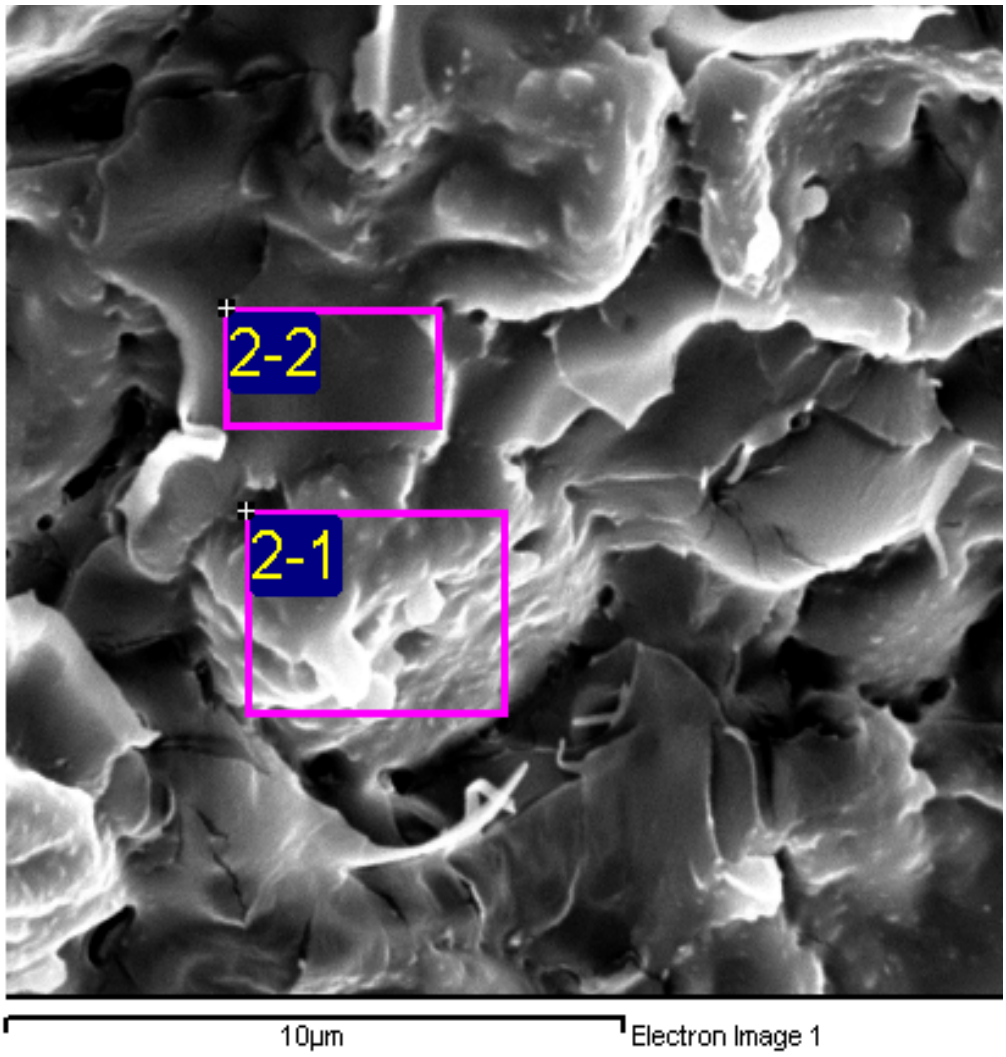

Figure 5.16 SEM image of Pt/Pd shadowed fracture surface for 15% AOT 0% water sample showing smooth fracture surface and hemispherical depressions having a rough surface texture.

These hemispherical depressions were of the order of 1-2 microns in diameter. Further examination of the smooth surface by energy dispersive x-ray elemental analysis shows that the smooth regions were totally devoid of sulfur or sodium. On the contrary, both of these

elements were found in the hemispherical depression regions. This phenomenon suggests microphase separation AOT during polymerization. The result can explain the turbidity of the 15% AOT 0% water sample, which looks almost the same as the 30/70 AOT/MMA 0% water rod illustrated in Figure 5.2. The turbidity of the samples containing water can therefore be unequivocally ascribed to microphase separation of the surfactant AOT during polymerization. This microphase separation into spheroidal domains is most likely into vesicular structures, since AOT is known to favor lamellar mesophase formation.

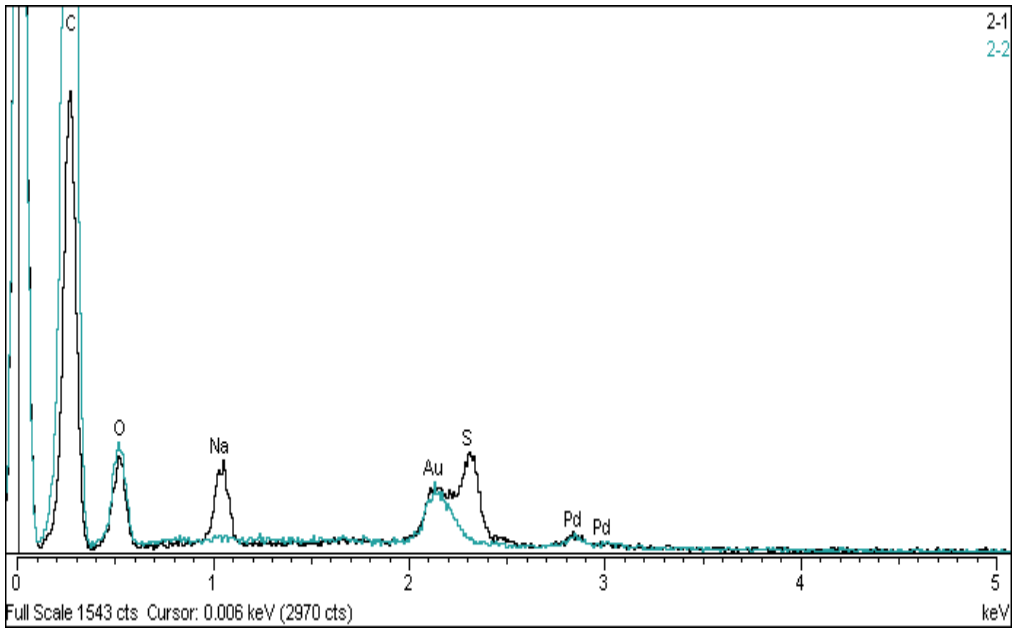

Figure 5.17 Energy dispersive x-ray elemental analysis for the fractured surface showing that the smooth region (2-2 in Figure 5.16) is totally devoid of sulfur or sodium and both of these elements present in the hemispherical depression regions

5.2.6 Ignition Test

Several 30/70 AOT/PMMA samples were examined for fire-resistance by a modified form of the UL 1581(VW1) ignition test. [4] Samples produced in culture tubes were placed at the blue flame tips generated by a Fisher burner to ignite the samples, and then removed from the flame to see if the combustion would be sustained. The results are illustrated in Figure 5.18.

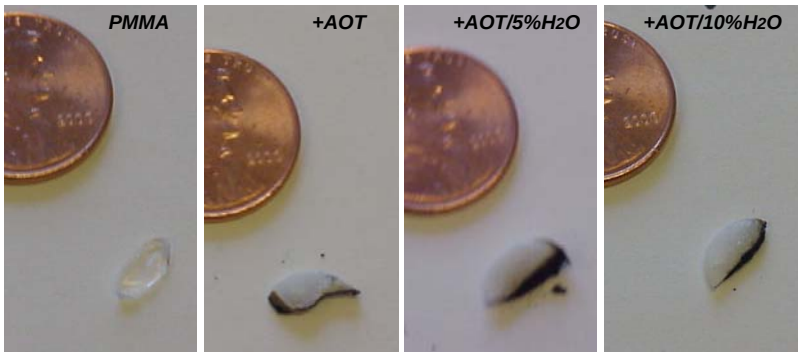

Figure 5.18 Ignition test results for 30/70 AOT/PMMA with 0, 5, 10% water, along with PMMA control and AOT.

The PMMA control burned cleanly and continuously. AOT itself, when held in the flame as the polymer samples were held, would not ignite. The compound would melt and drop into the burner prior to ignition. The AOT containing samples can be ignited, but burn slowly and the

combustion often would self-extinguish. The presence of AOT in the polymer samples accounts for this combustion or ignition resistance of the AOT/PMMA samples.

REFERENCE

1. Brun, M; Lallenmand, A.; Quinson, J. F.; Eyraud, C. *Thermochim. Acta* **1977**, 21, 59.
2. Quinson, J. F.; Mameri, N; Guihard, L.; Bariou, B. *J. Membr. Sci.* **1991**, 58, 191.
3. Nakao, S. *J. Membr. Sci.* **1994**, 96, 131.
4. K.L. Tannehill, Inc. Web Site. http://www.kltannehill.com/technical Documents/Cable Flame Test.htm (accessed August 20, 2004).

CHAPTER 6

POLYMERIATION OF MDOS SYSTEMS AND CHARATERIZATIONS

Polymerizable surfactants have been reported that they are capable of preserve the interfacial network of the microstructure during polymerization. [1-4] So, it is possible to make transparent nano-porous materials from reverse microemulsion systems with polymerizable surfactant.

6. 1 POLYMERIZATION

6.1.1 Polymerizations in the L_2 Domain of Water/MDOS/MMA System

Reverse microemulsions of the water/MDOS/MMA system were thermally polymerized in sealed 5mm O.D. diameter NMR tubes at 70°C in an oil bath for 4~6 hours. AIBN was pre-dissolved in the MMA and was used as initiator at 0.1 and 1 wt% of MMA plus MDOS.

Polymerization temperature was not the same as the temperature at which phase diagram was investigated. It is important to verify the L_2 domain at this temperature. Therefore, we traced a very schematic L_2 domain of water/MDOS/MMA system at 70°C to see the effects of temperature on the L_2 boundary. The 70°C boundary of the L_2 domain is illustrated in Figure 6.1.

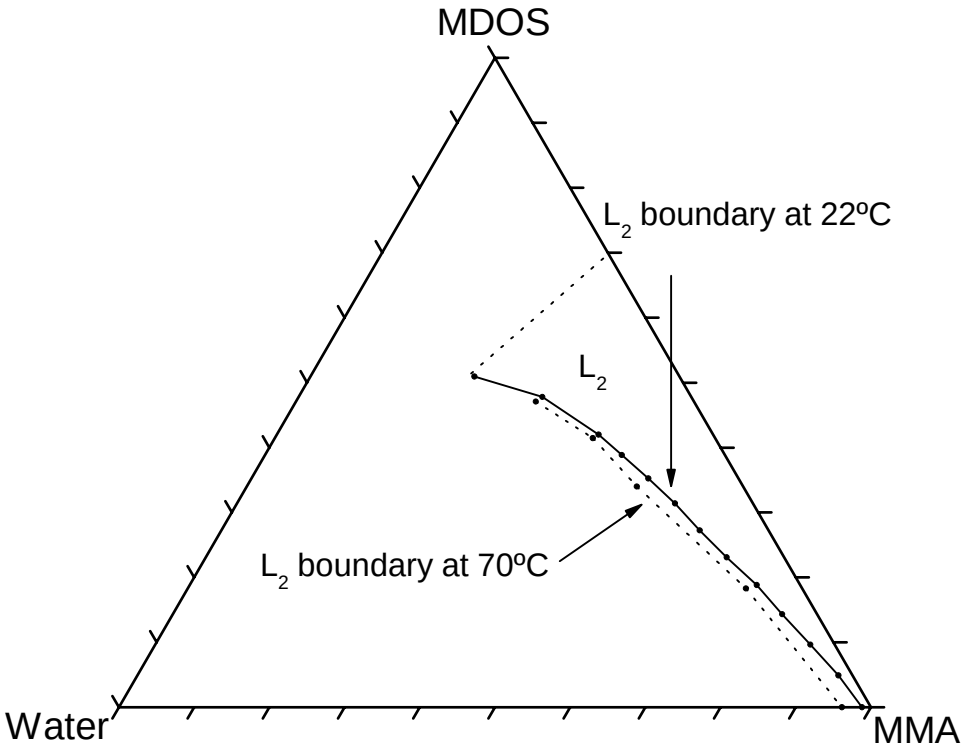

Figure 6.1 Schematic L_2 domain of water/MDOS/MMA system obtained at 70°C and at room temperature 22±1°C. The L_2 domain at 70°C is slightly larger.

The microemulsions were prepared with compositions very close to the L_2 boundary obtained at room temperature in PTFE-lined screw-capped culture tubes. The microemulsions were then immersed in an oil bath at 70°C for about 20~30minutes to insure phase equilibrium. If the microemulsion was still optically transparent, it was then cooled down to room temperature and a calculated amount water was added to increase the weight fraction of water by about 1wt% and it as then placed back in the oil bath at 70°C. This process was repeated until persistent turbidity was obtained at 70°C. It appears that the L_2 domain increases slightly when temperature is increased. The extent of increase over lower MDOS concentration is greater than at higher MDOS concentration. It turns out that at polymerization temperature, the L_2 domain was slightly expanded.

Two compositional segments at 20/80 and 40/60 MDOS/MMA where polymerizations were conducted are illustrated in Figure 6.2. These reverse microemulsions for polymerization were formulated with 0, 5 and 10 wt% water.

After 4 hours of polymerization 70°C, optically transparent rods were recovered by breaking the NMR tubes. The pictures of rods so obtained are shown in Figures 6.3 and 6.4. It is quite interesting to see that those surfactant-containing polymer rods are transparent with very week turbidity as compared with the PMMA control sample. The photographs

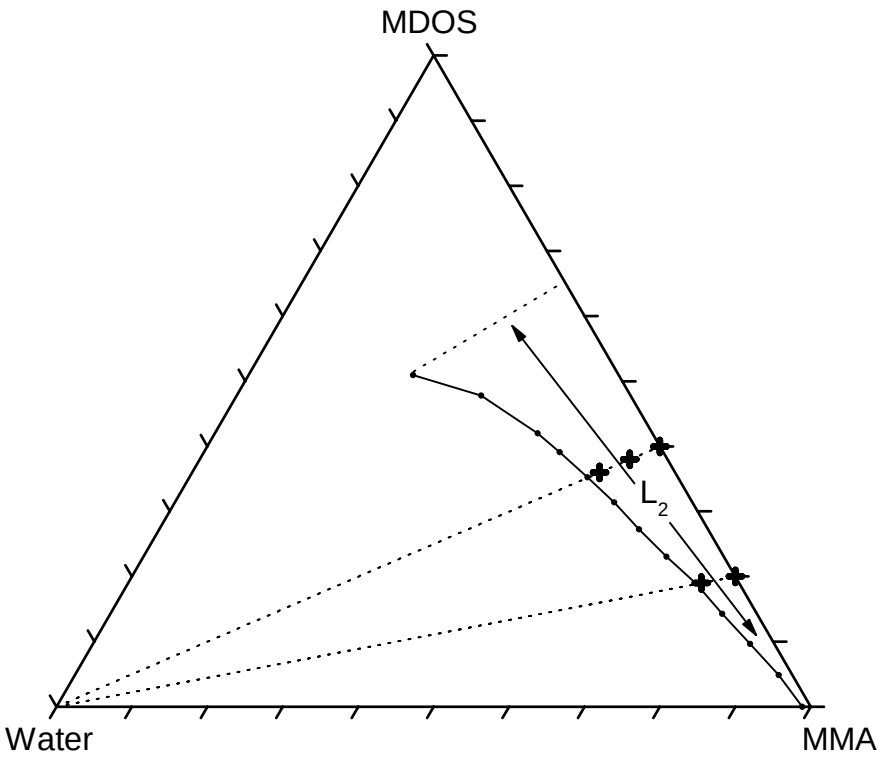

Figure 6.2 Loci of reverse microemulsion polymerizations along the 20/80 and 40/60 MDOS/MMA.

were taken with a black background to highlight the slight turbidity of the surfactant containing samples. When being observed in regular illumination, the turbidity can hardly be distinguished.

The turbidity appears to increase when weight fraction of water is increased. This phenomenon is similar to the Tyndall effect which is caused by scattering of visible light by very small particles suspended in

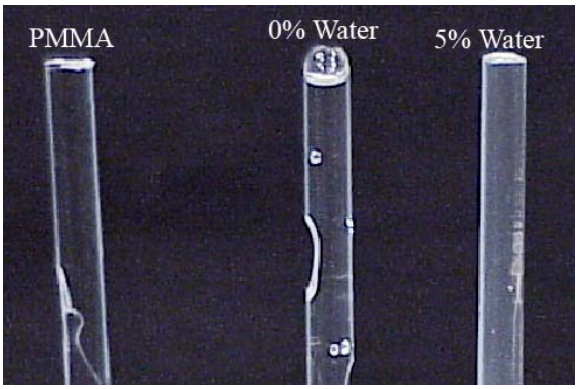

Figure 6.3 MDOS/PMMA samples polymerized at 70°C. The compositions were formulated at 20/80 MDOS/MMA with 0, 5 wt% water.

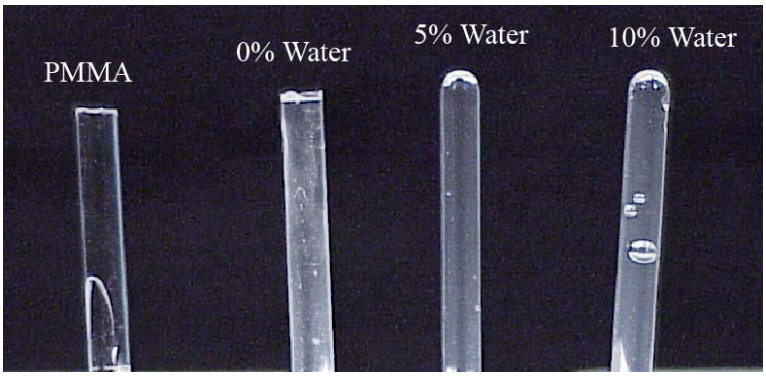

Figure 6.4 MDOS/PMMA samples polymerized 70°C. The compositions were formulated at 40/60 MDOS/MMA with 0, 5, and 10% water.

a transparent medium. Pavel et al also reported transparent solid obtained from didecyldimethylammonium methacrylate/MMA/water system which also had a weak Tyndall effect. And SEM image showed the presence of 15~20nm particles in the PMMA matrix. [5]

Water/MDOS/MMA reverse microemulsions were also formulated with 10/90, 20/80, 30/70, 40/60, 50/50, and 60/40 MDOS/MMA ratios, and weight fractions of water that were 1, and 2% less than corresponding L_2 boundary points. These formulations were polymerized at 70ºC and a schematic clear domain after polymerization was obtained. This clear domain is illustrated in Figure 6.5. Nearly the entire L_2 domain in this MDOS system yields optically clear composites after thermally initiated polymerization.

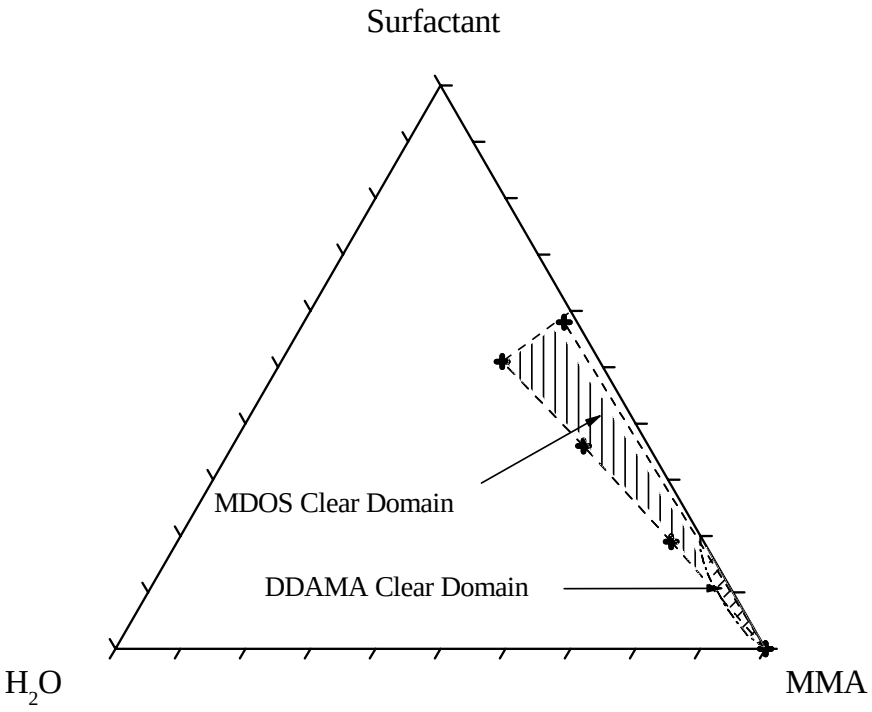

Figure 6.5 MDOS L_2 domain that produces clear composites is nearly the entire L_2 domain in the water/MDOS/MMA system. This domain of DDAMA is much smaller. [5]

Pavel and Mackay used didecyldimethylammonium methacrylate (DDAMA), a polymerizable surfactant, in the water/DDAMA/MMA ternary system and reported a quite large L_2 domain. Thermally initiated polymerizations in this domain were carried out at 50°C using BPO as initiator and optically clear nanocomposites were reported (This domain is also illustrated in Figure 6.5 along with the clear domain for MDOS). Without water Pavel reported that clear polymer phase was obtained up to 35% DDAMA. [5] We found in the water/MDOS/MMA system considerably larger "optically clear" domain, even though the starting L_2 domain in our system is much smaller.

6.1.2 Polymerization in L_2 of Aqueous Acrylamide/MDOS/MMA System

Polymerizations in 10 and 20% aqueous acrylamide/MDOS/MMA reverse microemulsions were conducted at 70°C in 5mm O.D. NMR tubes. AIBN was pre-dissolved in MMA and was used at 0.1 and 1% by weight of MMA and MDOS. Clear solid rods were produced with microemuliosons formulated at 10/90, 20/80, 30/70, 40/60, 50/50 and 60/40 MDOS/MMA and aqueous phase weight fraction was very close to the corresponding L_2 boundary points. Similarly to the results obtained from water/MDOS/MMA system, clear polymers were produced over nearly the entire L_2 domain. At the 40/60 MDOS/PMMA ratio with 15.5% of

10% aqueous acrylamide, the corresponding rod is illustrated in Figure 6.6 along with a 40/60 MDOS/PMMA 14% water rod. Though the total weight fraction of water is almost the same, the 15.5% (10% aqueous acrylamide) sample appears to have greater transparency.

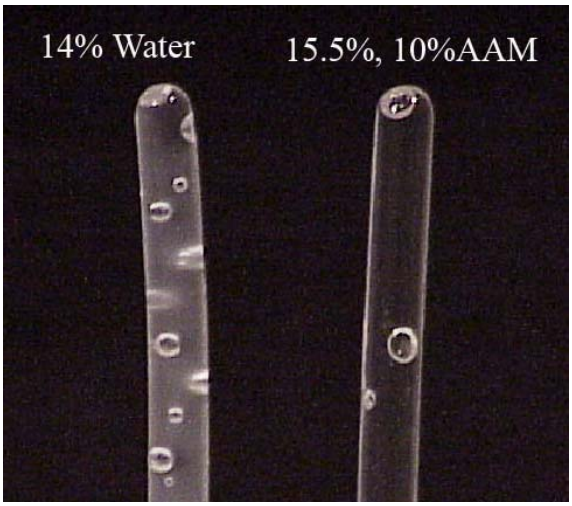

Figure 6.6 Water-MDOS sample and 10% aqueous acrylamide-MDOS sample.

6.1.3 Polymerization of Water/MDOS/(1:4 EGDMA/MMA) System

Ethylene glycol dimethacrylate (EGDMA) is cross-linking monomer. Its presence can slightly expand the L_2 domain. Microemulsions formulated within the L_2 domain were also thermally polymerized using 5mm O.D. NMR tubes at 70°C for 4 hours. AIBN was pre-dissolved in MMA and was used at 1% by the total weight of monomers and surfactant.

Reserve microemulsions formulated with 20/80 MDOS/(1:4 EGDMA/MMA) and 0, 5, or 10wt % water produced optically transparent rods. These rod have similar physical appearances to those shown in Figures 6.3 and 6.4.

6.1.4 Polymerization of Water/MDOS/7:3 MMA/HEMA-5% EGDMA)

As we know from Chapter 4, HEMA can slightly enlarge the L_2 domain of the water/MDOS/MMA. Microemulsions formulated in this L_2 domain were also thermally polymerized in 5mm O.D. NMR tubes at 70°C. AIBN was pre-dissolved in MMA and was used at 1% by the total weight of monomers and MDOS.

Reserve microemulsions formulated with 20/80 MDOS/7:3 MMA/HEMA-5% EGDMA and 0, 5, or 10 wt% water produced optically transparent rods. These rods have similar physical appearances of those as shown in Figures 6.3 and 6.4. An extra formulation was polymerized with 40/60 MDOS/7:3 MMA/HEMA-5% EGDMA and 14% water. This composition is right on the L_2 boundary. The polymer rod obtained is more turbid than the others. The polymer rods obtained from the 40/60 MDOS/7:3 MMA/HEMA-5% EGDMA microemulsion series are illustrated in Figure 6.7.

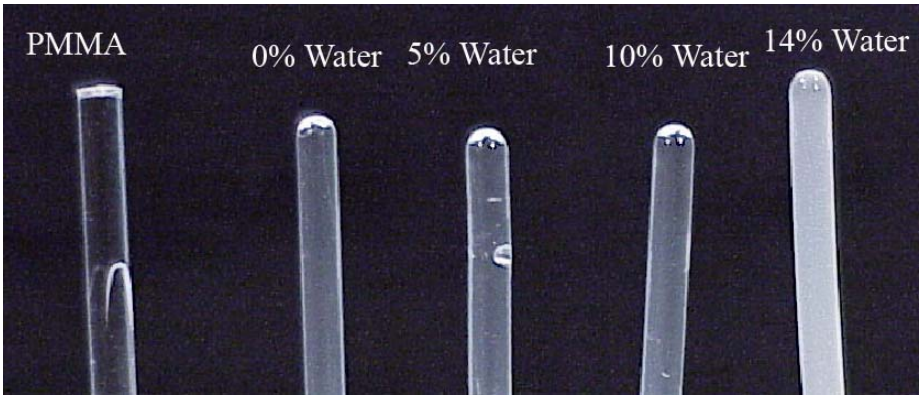

Figure 6.7 40/60 MDOS/(7:3 MMA:HEMA with 5% EGDMA) samples formulated with 0, 5, 10, and 14% water photographed along with PMMA. Clear-Tubid transition is between 10% and 14% water.

6.2 CHARACTERIZATIONS

6.2.1 Thermostability

As described in the Chapter 2, thermal stability was analyzed using TGA in air or N_2 over room temperature to 600°C interval with a 10°C per minute heating rate. Weight loss profile of 20/80 MDOS/PMMA samples that were shown in Figure 6.2 are plotted in Figure 6.8.

The PMMA control sample decomposes over the 240-350°C range. The decomposition of all MDOS-containing samples commences at about the same temperature. The MDOS samples are thermally more robust than

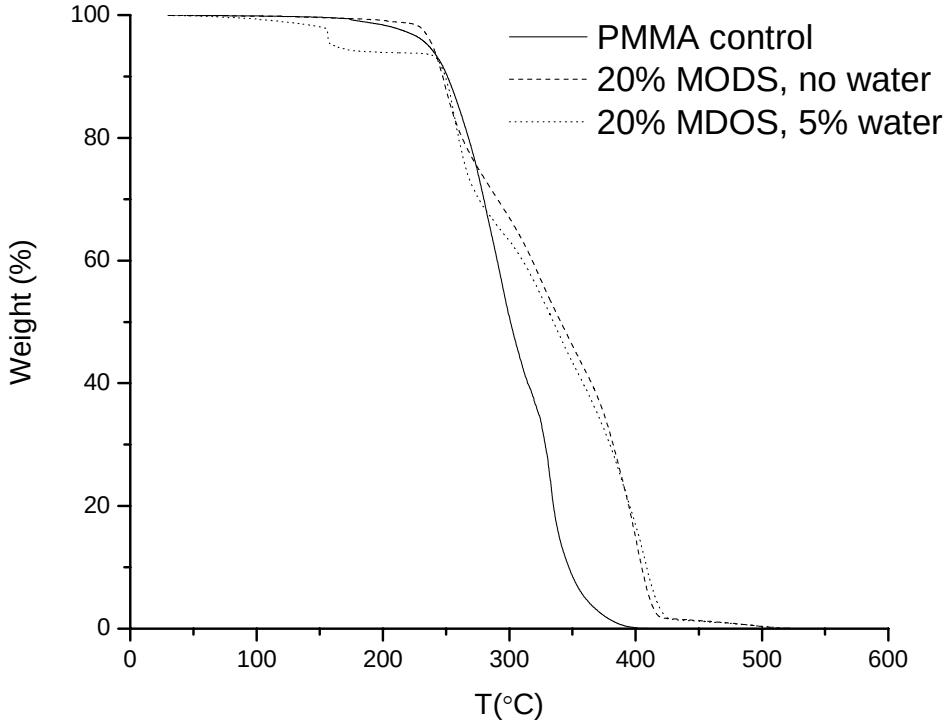

Figure 6.8 Weight loss of 20/80 MDOS/PMMA samples with 5 wt% water in air. PMMA and 20/80 MDOS/PMMA are control samples.

PMMA over 285~420°C and decompositions deviate to a slower rate than the PMMA control. This deviation can be assigned to the presence of MDOS, as MDOS decomposes over the 300~500°C (Figure 3.4). The last 10-12% of MDOS remnant requires a further 150°C of activation (350-500°C), and this remnant is clearly seen in the main part of the figure and corresponds to the last 2-3% loss over the 410-510°C interval.

The overall weight loss curves of poly(MDOS/MMA) sample almost overlap with that of the PMMA control until the MDOS-containing sample deviate to a slower decomposition rate at about 285°C. The 5% water MDOS/PMMA sample does not begin to loss weight until the temperature reaches about 100°C. The first 2% water is gradually released until it releases about 2% more water in a few degrees interval around 160°C. The remaining 1% water diffuses out gradually until the sample starts to decomposition. The 5% weight loss of this sample before decomposition agrees with the microemulsion formulation. It is obvious that the weight loss can be primarily ascribed to the release of water, but not to release of un-reacted monomer since such weight loss is not seen in the poly(MDOS/MMA) sample and the PMMA control.

These samples were also analyzed under N_2 atmosphere. The results are illustrated in Figure 6.9. It was as expected that the rate of decomposition would be slower than that in air. The poly(MDOS/MMA) samples and the PMMA control decompose at a slower rate.

40/60 MDOS/(1:4 EGDMA/MMA) samples were analyzed in air. The results are shown in Figure 6.10. The gradual release of water agrees with the total in the corresponding microemulsion formulation. Weight loss behavior is similar to that of poly(MDOS/MMA) samples illustrated in Figure 6.7.

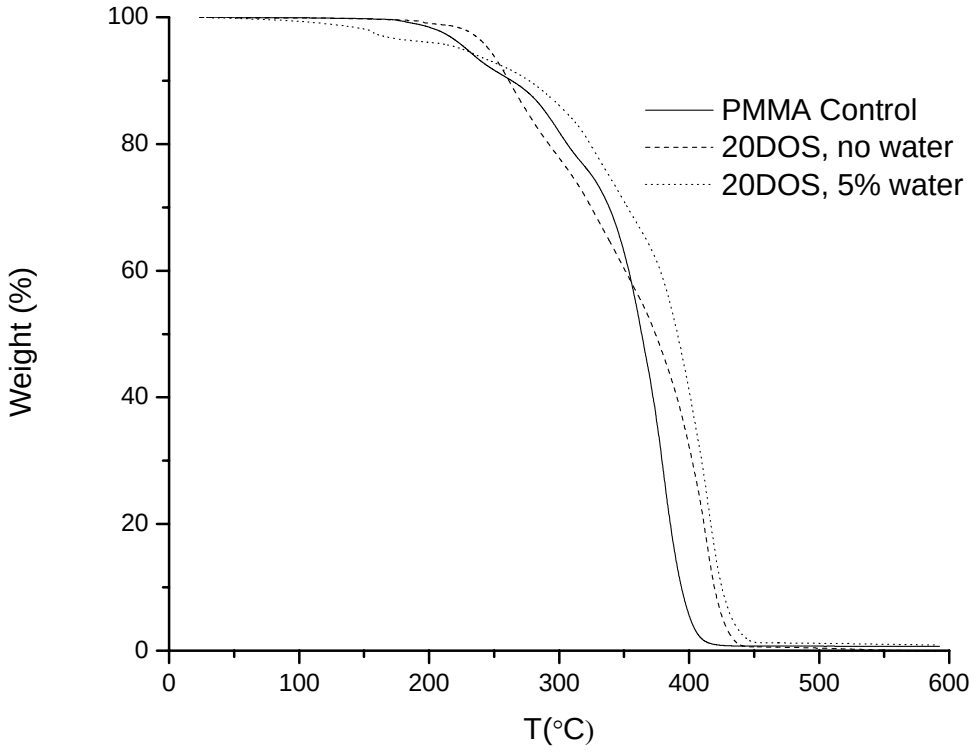

Figure 6.9 Weight loss 20/80 MDOS/PMMA samples with 5wt% water in N_2. PMMA and 20/80 MDOS/PMMA are control samples.

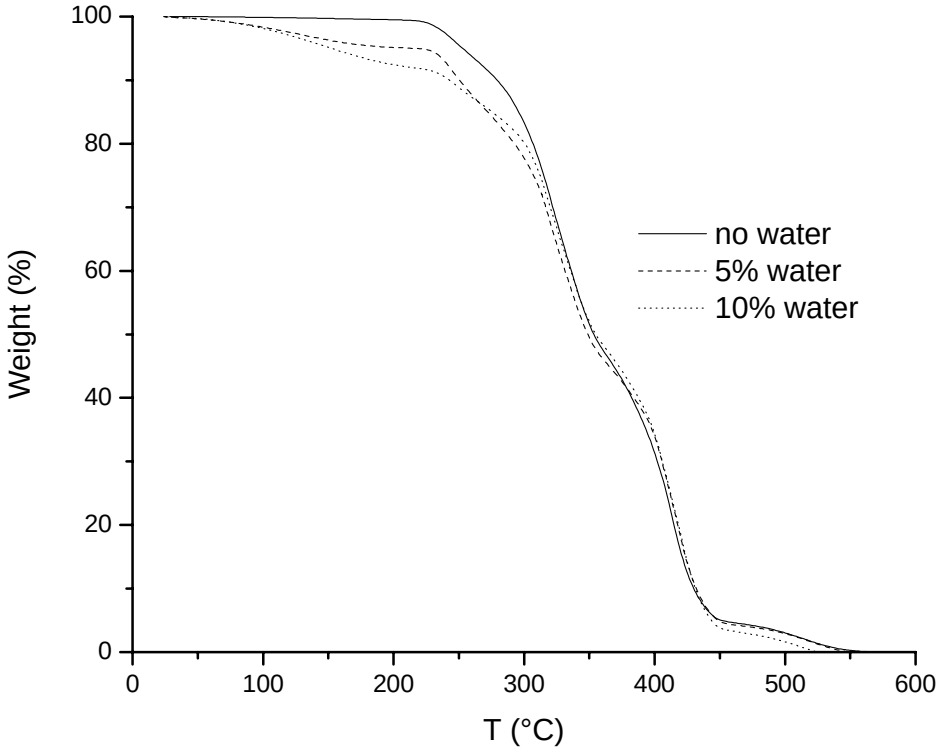

Figure 6.10 Weight loss of polymerized 40/60 MDOS/(1/4 EGDMA/MMA) samples with 0, 5 and 10 wt% water in air

Samples illustrated in Figure 6.6 were also analyzed. These two samples contain about equal amounts of water. The TGA data are in shown in Figure 6.11.

The weight loss curves of the two samples essentially overlap prior to the onset of decomposition. About 4% water is gradually released over the room temperature to 130°C interval. The water release rate sharply rises

and about 6% water is released over 130~150ºC interval. The rest of water diffuses out starting at from 150ºC until decomposition of polymer commences.

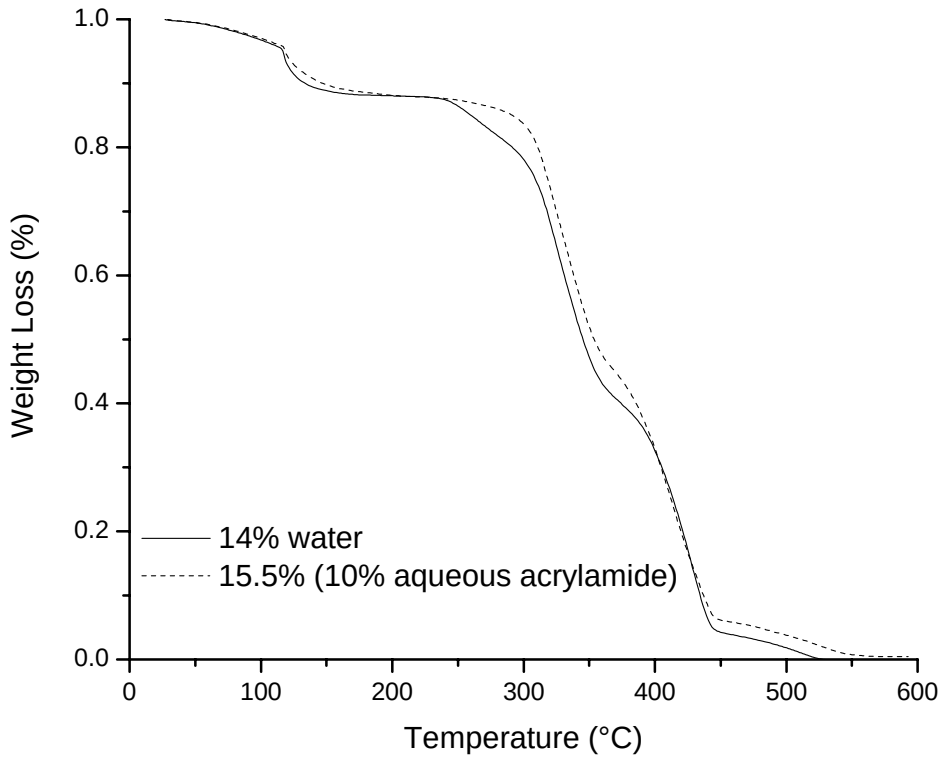

Figure 6.11 Weight loss of polymerized 50/50 MDOS/MMA with 14% water and 50/50 MDOS/MMA with 15.5% of 10% aqueous acrylamide in air. The two samples contain almost amount of water.

The water release behavior of MDOS/MMA-copolymer nanocomposites is obviously different than that of AOT/PMMA materials. The sharp rise of water release rate around 150ºC suggests that water is confined in some microstructures, perhaps nano-droplets that were formed prior to

polymerization and were captured by polymerization. The clarity of the samples suggests that microphase separation did not occur during polymerization. The sizes of nano-droplets are small enough so they do not cause turbidity.

6.2.2 Molecular Weight

The molecular weight of samples formulated with 10/90~60/40 MDOS/MMA was analyzed as described in Chapter 2. The molecular weight analysis was done using 1,1,1,3,3,3-hexafluoroisopropanol (HFIP)/0.01M tetraethylammonium nitrate as eluent. [6] The results were interpreted in a letter from Dr. Thomas Mourey to Dr. John Texter and are summarized in Table 6.1 and illustrated in Figure 6.12~6.14.

Table 6.1 Molecular Weight Analysis of PMMA Control and of MDOS/MMA Copolymers

MDOS/MMA	log M_n[a]	log M_w[b]	log M_z[b]
PMMA	4.98	5.73	6.09
10/90	5.09	5.82	6.15
20/80	5.16	6.02	6.35
30/70	5.28	6.03	6.36
40/60	5.32	6.11	6.41
50/50	5.48	6.26	6.51
60/40	5.62	6.23	6.51

[a] Viscometry detection and universal calibration.

[b] Two angle light scatting detection.

The best number-average molecular weight values come from SEC-viscometry detection and universal calibration.(a). The viscometer is more sensitive than light scattering detection to the smallest polymer molecules, and the smallest polymer molecules have the greatest influence on M_n. The light scattering detector (b) is best for measuring the weight-average and *z*-average molecular weights because some of the molecules are too large for the SEC column set and fall outside of the universal calibration curve. Radius of gyration (*z*-average) is from light scattering, and the intrinsic viscosity was measured by the viscometry detector. All of the "best" values from the different detection methods are summarized in Table 6.1. The results for M_n, M_w and M_z of the PMMA control are consistent with the result in Table 5.1. log M_n, log M_w, and log M_z are plotted vs weight fraction of MDOS in Figures 6.12~6.14. The correlations appear to be linear. It turns out that the weight of MDOS has a great impact on molecular weight.

The molecular weight distributions overlaid in Figure 6.15 indicate that the distributions creep up to higher masses as more MDOS co-monomer is included. The regions beyond 10^6 are distorted for several reasons, and it is difficult to make quantitative comparisons of distribution shapes. The distortions will likely bias the weight-average and *z*-average molecular weight averages low. The inset in Figure 6.15 shows the PMMA, 30/70 and 60/40 MDOS/MMA copolymer samples plotted as log M vs.

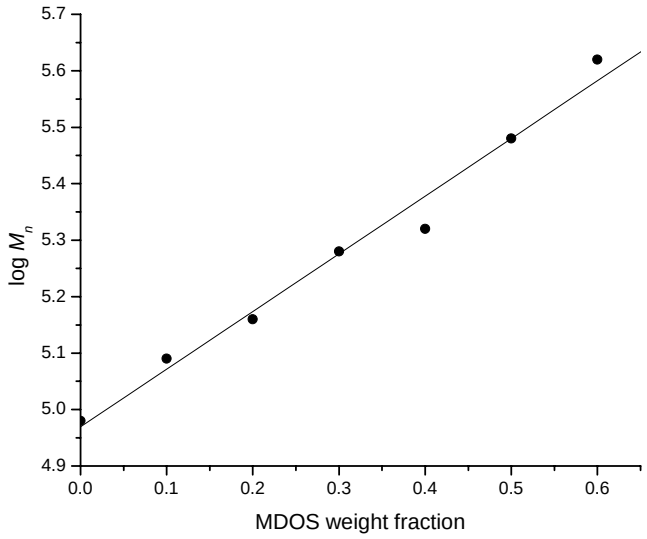

Figure 6.12 Log M_n for poly(MDOS/MMA) vs. MDOS weight fraction

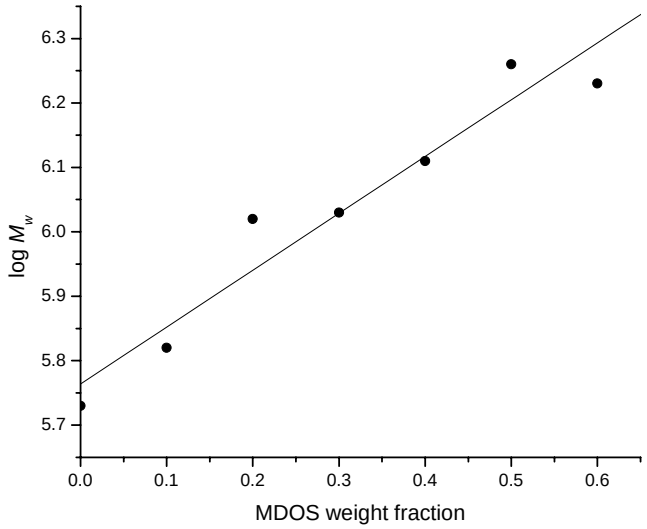

Figure 6.13 Log M_w for poly(MDOS/MMA) vs. MDOS weight fraction

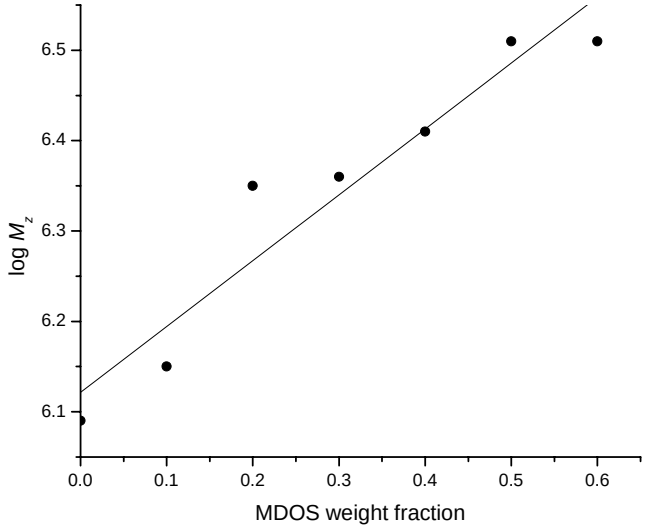

Figure 6.14 Log M_z for poly(MDOS/MMA) vs. MDOS weight fraction

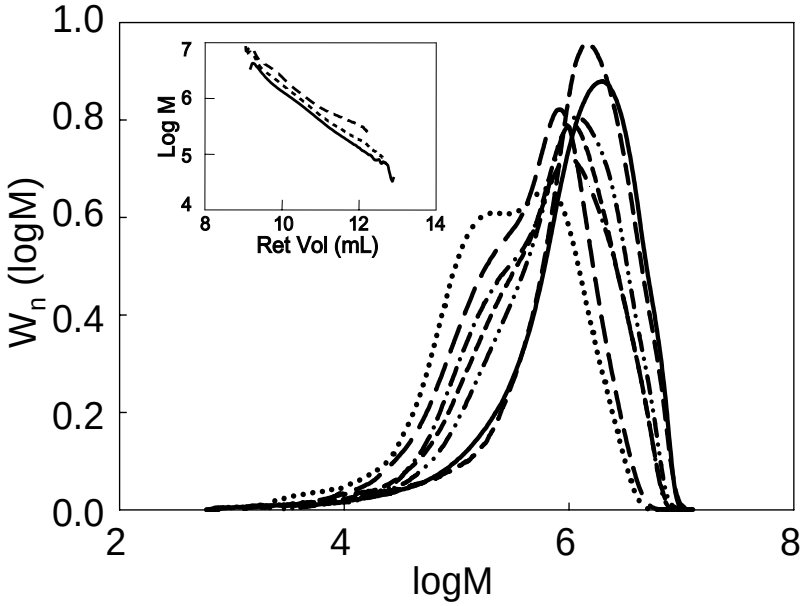

Figure 6.15 Molecular weight distribution of poly(MDOS/MMA)

retention volume. Molecules at the same retention volume have the same hydrodynamic size.

These results suggest that the increase in mass with increasing MDOS content for equivalent size molecules is as a result of the high mass of the MDOS monomer compared to MMA, although there could be changes in conformation as well; high MDOS-content chains may be more compact (globular) in this polar HFIP eluant than 100% PMMA. The bis(2-ethylhexyl)suofosuccinate counterion would be expected to induce clustering and intrachain micellization and is consistent with compaction.

REFERENCE

1. Gan, L. M.; Chieng, T.H.; Chew, C. H.; Ng, S. C. *Langmuir* **1994**, 10, 4022.
2. Li, T. D.; Gan, L. M.; Chew, C. H.; Teo, W.K.; Gan, L. H. L*angmuir* **1996**, 12, 5863.
3. Chew, C. H.; Li, T. D.; Gan, L. H.; Quek, C. H.; Gan, L. M. *Langmuir* **1998**, 14, 6068.
4. Challa, V.; Luta, K.; Lopira, S.; Cheung, H. M.; von Meerwall, E. *Langmuir* **2003**, 19, 4154.
5. Pavel, F. M *Polymer Blend and Polymer/Nanoparticle compostites From Microemulsion, Doctorate Dissertation* **2001**.
6. Mourey, T. H.; Bryan, T. G. *J. Chromatogr. A.* **2003**, *36*, 2674.

CHAPTER 7

CONCLUSIONS AND FUTURE WORK

A couple of surfactants, MDOS, ADOS, Ag(AOT), $Zn(AOT)_2$, sodium bis(2-ethylhexyl) phosphate were synthesized and their properties were analyzed. They were used in investigating reverse microemulsion polymerization of systems containing aqueous phase, surfactant, and monomer.

Systems with different surfactants yielded polymer samples with quite different optical and mechanical properties. L_1 and L_2 domains of water/AOT/MMA were investigated. L_2 domain increases dramatically around AOT/MMA ratio of 50/50. Opaque polymer rods were obtained from various AOT compositions, even though the starting reverse microemulsions were transparent. The length scales, over which water-PMMA micro-phase separation occurs, decrease as water content and surfactant content decrease. Both water and surfactant appear to provide flame and ignition resistance. L_1 and L_2 domains of similar microemulsion systems with the hydrophilic monomer acrylamide in the aqueous phase and with or without the cross-linking agent ethyleneglycol dimethacrylate have been studied. The presence of acrylamide in the aqueous phase expands the L_2 domain towards the

water corner. The L_2 and L_1 domains connect at 40/60 AOT/MMA when acrylamide is 20 wt%. Free radical polymerizations were also conducted with these systems. Only opaque or translucent rods with obvious evidence of micro-phase separation were recovered. Phase separation in all cases occurs at an early stage of polymerization, approximately 20 minutes after polymerization starts. TGA weight loss profiles of the opaque or translucent rods under nitrogen and air indicates water that is entrapped in is consistent with the compositions of starting inverse microemulsions. Perhaps phase separation is due to AOT being less soluble in polymer/monomer mixtures. SEM image also convinced phase separation. DSC thermoporosity measurements showed that a portion of water was confined in micro-structure in nanometer length scale which caused melting point depression of water.

MDOS (2-Methacryloyloxy)ethyl trimethylammonium bis(2-ethylhexyl) sulfosuccinate, were synthesized by ion exchange methods. This surfactant has polymerizable cation and double-tail anion. Partial phase diagrams of MDOS systems were studied. L_2 domain of water/MDOS/MMA is pretty large. Free radical polymerizations were conducted within L_2 domain and in the adjacent two phase emulsion domain in order to entrap water droplets. Optically transparent polymer composites were obtained from almost the entire L_2 domain of these systems. Translucent polymers were also obtained with a starting system

in the adjacent two phase emulsion region. Compared with the water/AOT/MMA system, the length scales, over which water-PMMA phase separation occurs decrease dramatically. Cross-linking, hydrogel, and surfactant polymerization variations were examined with a view towards further understanding of factors that control phase separation (and transparency) on meso- and nano-lengthscales. Similar polymerizations were conducted with 10, and 20wt% aqueous acrylamide with 5 wt% cross-linking agent ethyleneglycol dimethacrylate. Transparent polymers are achieved in all cases with MDOS. TGA weight loss convinced that water in the samples is consistent with original formulation. Transparent material was successfully made from reverse microemulsion of MDOS systems with up to 14% water.

In terms of future work, methods of making ADOS, Ag(AOT), Zn(AOT), and sodium bis(2-ethylhexyl) phosphate need to be improved. Phase diagram and polymerization of systems containing these surfactants need to be studied. The combination of the above moieties and MDOS are possible to make antimicrobial, anti-corrosion composites material for varieties of applications.